Soft Matter

PAPER

View Article Online
View Journal | View Issue

Cite this: *Soft Matter*, 2024, **20**, 4434

Anionic starch-based hybrid cryogel-embedded ZnO nanoparticles: tuning the elasticity and pH-functionality of biocomposites with dicarboxylic acid units†

Sena Ciftbudak[a] and Nermin Orakdogen *[b]

Weakly anionic semi-interpenetrating polymer network (semi-IPN) biocomposites based on starch (ST)-incorporated poly(acrylamide-*co*-itaconic acid)/ZnO (ST-PAI/ZnO) were synthesized by a simple one-pot method *via* free radical aqueous polymerization. Hybrid biocomposites exhibited lower equilibrium swelling compared with neat copolymer gel. For both hydrogels and cryogels, swelling followed a decreasing order as copolymer PAI > starch-free PAI/ZnO > ST-PAI/ZnO gels. With the addition of 9% ST and ZnO, the swelling ratio of gels decreased from 898 to 68.3, resulting in a significant increase in elastic modulus. Compared with a fixed amount of ST, biocomposite cryogels exhibited significantly higher modulus than hydrogels. With the addition of 9% ST, the elastic modulus of cryogels reached 22.2 kPa while it was 2.7 kPa for the hydrogels. An equation expressing the effective cross-linking density of semi-IPNs presented by a cubic polynomial as a function of starch was obtained. As pH increased with the presence of dicarboxylic acid units, a gradual increase in swelling occurred at two different pH values. A gradually reproducible swelling change of semi-IPNs was depicted with pH ranging from 2.1 to 11.2. Biocomposite cryogels showed rapid swelling in a buffer solution of pH 11.2 and rapid shrinking in pH 2.1. Salt-induced swelling testing showed that the ability to reduce the degree of swelling and solubility of starch was $Br^- > Cl^- > NO_3^- > SO_4^{2-}$ for anions consistent with the Hofmeister series. Adsorption efficiency for the removal of methyl violet (MV) dye was analyzed using Langmuir, Freundlich, Dubinin–Radushkevich and Temkin isotherm models. The results confirmed that the Langmuir isotherm and pseudo-second-order model are suitable for describing MV adsorption on semi-IPN biocomposites. The synthesized biocomposites with good swelling/deswelling kinetics in different pH-buffer solutions, high saline absorbency, desirable adsorption efficiency, and acceptable pH-dependent swelling reversibility can be considered as smart hybrid materials for the adsorption of the dye in water purification tasks.

Received 28th January 2024,
Accepted 9th May 2024

DOI: 10.1039/d4sm00136b

rsc.li/soft-matter-journal

Introduction

Natural polymer-doped gel synthesis has begun to receive increasing attention in hybrid material design owing to its biocompatibility, hydrophilicity, and biodegradability.[1–3] Compared with synthetic polymer-based gels, starch-containing hybrid materials have advantages of green synthesis, such as being a renewable resource, economically feasible, adaptable in structure and composition, and meeting the requirements of worldwide environmental and health concerns. Starch consists of a number of monosaccharide or glucose molecules linked together with α-D-(1–4) and α-D-(1–6) linkage(s).[1,2] The two main structural components of starch are amylose and amylopectin having the same repeating units that are linked in linear and branched ways. The amylose content and the polymerization temperature are two optimum parameters in the starch-based gel-synthesis. In addition, the numerous hydroxyl groups of each glucose residue make starch both hydrophilic and amenable to modifications. Some hydroxyl groups in starch chains can react with di- or multifunctional crosslinkers, leading to covalent crosslinking of starch. With the hydroxyl groups in the backbone, it is possible to easily incorporate cationic or anionic functional groups into starch that can vary the solution viscosity and association behavior to prepare modified starch-based gels with inexpensive reagents.

The graft copolymerization of vinyl monomers on starch in the presence of a crosslinker has become a promising method

[a] *Graduate School of Science Engineering and Technology, Department of Chemistry, Istanbul Technical University, Maslak, Istanbul, 34469, Turkey*
[b] *Department of Chemistry, Soft Materials Research Laboratory, Istanbul Technical University, Maslak, Istanbul, 34469, Turkey. E-mail: orakdogen@itu.edu.tr; Tel: +90-212-2853305*

† Electronic supplementary information (ESI) available. See DOI: https://doi.org/10.1039/d4sm00136b

for designing polysaccharide-based hydrogels with desirable properties in practical applications. In graft copolymerization, –OH groups on the saccharide units and the initiator form redox pair-based complexes, initiating the graft polymerization of vinyl monomers and crosslinkers on the polysaccharide chains.[1] The mechanism of grafting acrylamide (AAm) onto starch in the presence of Ce^{4+} as a free radical initiator was suggested by Dragan and Apopei to prepare semi-IPN hydrogels consisting of polyacrylamide (PAAm) and natural potato starch as the matrix.[2] The approach to achieve superior mechanical strength in polymer hydrogels *via* starch-reinforced strategy in functional soft material design with the combination of starch and hydrophilic polymers was reported by Shang and co-workers.[3] Chemically and physically crosslinked hybrid double networks containing starch with an elastic modulus of ~29.7 kPa were developed to form strong dynamic interactions within the gel matrix. By a simple method, cassava starch was introduced into chemically crosslinked hydrogels based on poly(acrylic acid) and 2-acrylamido-2-methyl-1-propanesulfonic acid. After crosslinking with *N*,*N*-methylenebis acrylamide (BAAm), the formation of a hybrid composite containing a covalent network, starch gelatinization and ethanol treatment led to the formation of enhanced physical crosslinked interactions within the hydrogels. By the combination of graft polymerization and complex crosslinking, an effective method to increase the resistance and adhesion strength of starch-based adhesives was proposed. Jin and coworkers prepared starch-based adhesives by grafting itaconic acid (IA) and *N*-hydroxyethyl acrylamide (HEAA) onto corn starch.[4] Their results showed that starch grafted with IA and HEAA formed a complex crosslinked network as a result of crosslinking reactions after the heat treatment process. HEAA was grafted on the partial crosslinking sites of itaconic acid, which served as a backbone for further crosslinking of starch particles. In a recent study, environmentally friendly superabsorbent hydrogels based on starch and IA, which have great potential to be used in agricultural applications, were prepared by grafting AAc and IA on the starch backbone using a solution polymerization.[5] The grafted chains formed by donating macroradicals from the hydroxyl groups of starch to nearby AAc were combined with the end of the vinyl group of BAAm to form a 3D crosslinked structure. The swelling kinetics of hydrogels revealed faster water absorption with higher IA. Incorporating two or more materials in the composite matrix could combine the properties of those different materials with the unique characteristics of starch. Olad and coworkers proposed a synthetic pathway by grafting AAc and AAm onto the starch backbone in the presence of cellulose nanocrystals and poly(vinyl alcohol), as an interpenetrating network.[6] Their results revealed that by acting as a multifunctional crosslinker of cellulose nanocrystals, the nanocomposites exhibited a dramatic improvement in the compressive strength, and elastic modulus compared to neat hydrogel.

By combining the proposed synthetic pathways, starch (ST) containing weakly anionic hybrid gels embedded ZnO-nanoparticles were prepared using neutral monomer acrylamide (AAm) and anionic comonomer itaconic acid (IA), a biobased dicarboxylic acid carrying an acryloyl group, *via* the semi-IPN strategy. The choice of anionic IA was based on its green nature containing vinyl and two carboxyl groups produced by biological fermentation, as well as being a renewable monomer that can copolymerize with vinyl monomers such as AAm, providing pH-sensitivity to the gel structure.[7] The reason for embedding ZnO-nanoparticles into hybrid biocomposites is to provide antimicrobial properties. It was chosen due to its versatile nature, such as good adsorption capacity, large surface-to-volume ratio, high surface area, high catalytic efficiency, regulation of immune function, protein synthesis and cell division in the body.[8] The structural and morphological features of semi-IPN biocomposites depending on the amount of ST were examined by XRD. The amount of BAAm in the hybrid nanocomposite was fixed to evaluate the effect of varying ST amounts on the physicochemical and mechanical properties. The effect of incorporated ST on the equilibrium swelling and compressive elasticity was studied. Observations regarding the increasing effect of the amount of ST on the elastic modulus and its decreasing effect on the swelling are presented comparatively for biocomposites. The swelling of semi-IPN biocomposites was measured in buffer solutions at a pH interval of 2–11.2. Furthermore, saline absorbency, compressive properties, pH-dependent swelling reversibility, on–off switching kinetics in different solutions, and capability for the adsorption of methyl violet dye from aqueous solutions were evaluated. Salt-induced swelling results of biocomposites with various starch content in sodium salts: NaBr, NaCl, $NaNO_3$ and Na_2SO_4 showed that the anions reduced the swelling degree of semi-IPN biocomposites in the order of $Br^- > Cl^- > NO_3^- > SO_4^{2-}$, consistent with the Hofmeister series.[9,10] The effect of contact time and dye concentration on the adsorption process efficiency was investigated. The Langmuir, Freundlich, Dubinin–Radushkevich (D–R) and Temkin isotherm models were used to describe the equilibrium behavior of the adsorption process. Pseudo-first-order, pseudo-second-order and Elovich models were used to study the kinetic behavior of the process. Systematic comparison of swelling and elasticity results will provide perspective on new hybrid material designs suitable for biological applications and adsorption studies.

Experimental

Materials

Acrylamide (AAm, ≥99%, Merck, Darmstadt, Germany), itaconic acid (IA, ≥99%, Sigma-Aldrich, Saint Louis, MO, USA), *N*,*N*-methylenebisacrylamide (BAAm, ≥99%) as a crosslinker, ammonium persulfate (APS, ≥98.0%) as an initiator and *N*,*N*,*N*,*N*-tetramethylethylenediamine (TEMED, ~99%) as a catalyst were purchased from Merck (Darmstadt, Germany) and used as received. High amylose corn starch (ST) with ≈70% amylose, Hylon VII, was supplied by Ingredion Germany GmbH. Based on the benefits of high amylose starch, it was specifically chosen to investigate the effect of amylose fine structures (branching structure and molecular size) on gel elasticity. Hydrochloric acid (HCl, Merck, 37%, Darmstadt, Germany), disodium hydrogen phosphate (Na_2HPO_4, ≥99.0%, Merck, Darmstadt, Germany), potassium

dihydrogen phosphate (KH_2PO_4, ≥99.0%, Riedel-de Haen, Germany), and sodium phosphate tribasic dodecahydrate ($Na_3PO_4 \cdot 12H_2O$, ≥98.0%, Merck, Darmstadt, Germany) were used for pH-dependent swelling testing. ZnO nanopowder was supplied by Sigma-Aldrich, Saint Louis, MO, USA. Sodium bromide (NaBr, ≥99.0%, Sigma-Aldrich, Saint Louis, MO, USA), sodium chloride (NaCl, ≥99.0%, Merck, Darmstadt, Germany), sodium nitrate ($NaNO_3$, ≥99.0%, Merck, Darmstadt, Germany) and sodium sulphate (Na_2SO_4, ≥99.0%, Merck, Darmstadt, Germany), were used for the salt-dependent swelling testing. Ultrapure water supplied by the MILLI-Q Laboratory system was used for the preparation of hybrid gels while distilled and deionized water were used in the swelling experiments.

Synthesis of starch-blended ZnO-embedded biocomposites

Hybrid starch-poly(acrylamide-*co*-itaconic acid)/ZnO, ST-P(AAm-IA)/ZnO, and biocomposite gels were synthesized by a simple one-pot method.[11] The aim was to investigate the effect of carboxyl groups of anionic comonomer IA and hydroxyl groups of ST on the hybrid gel properties such as the gelation temperature, pH-, temperature-, and salt-dependent swelling, dynamic swelling kinetics, compressive elasticity, and adsorption ability for the cationic dye MV. The amount of BAAm in the hybrid nanocomposite was fixed to evaluate the effect of varying ST amounts on the architecture and mechanical properties. Specifically, ST concentration was changed between 1.0 and 9.0% (w/v), while the amount of ZnO, the molar ratio of AAm/IA and the crosslinker BAAm were fixed in the pre-gel solution. Table 1 shows the synthesis sequence and nomenclature according to the varying amounts of ST. In order to obtain network structures with intact 3D integrity, the total monomer concentration C_0 in the gel structure was designed to be 5.32% (w/v), while the crosslinker ratio X (mole ratio of the crosslinker BAAm to the monomers AAm and IA) was kept at 1/80.

All hybrid gels were prepared using the following generalized easy procedure: ST was first dispersed in water (5 mL) and stirred for 1 h. A series of AAm/IA mixtures with a mol% ratio of 98/2 containing 0.12 g of ZnO was prepared by continuous mixing. 1.0 mL stock solution of BAAm (0.2766 g/20 mL water) and TEMED (750 μL/20 mL water) and then ST solution was added into this initial mixture. After the addition of 1.0 mL stock solution of APS (0.16 g/20 mL water), the common radical polymerization induced by the thermal initiator was conducted to prepare the hybrid gels. Each formulation was stirred for a total of 5 h before the polymerization reaction. Another point that makes the mixing procedure optimum is that the dispersion of ZnO becomes easier as the amount of ST increases after adding nanoparticles. The pre-gel solution was then transferred into several polypropylene syringes having a nominal capacity of 1.0 mL with an inner diameter of 4 mm and a length of 10 cm. The polymerization was performed at room temperature as well as at −18 °C for 48 h for the preparation of semi-IPN biocomposite hydrogels (Hgel) and cryogels (Cgel). The preparation procedure with the proposed mechanism for the formation of hybrid ST-PAI/ZnO gels is schematically illustrated in Scheme 1.

Table 1 Composition and designation of semi-IPN biocomposites crosslinked with BAAm in various ST content. ST (w/v)% = the mass/volume concentration of starch in the feed, and w_{gel} = gel fraction

Synt. order	ST-PAI/ZnO	ST (w/v)%	w_{gel} (Hgel)	w_{gel} (Cgel)
1	Copolymer PAI	0	92.55 (0.79)	93.10 (0.21)
2	ST0-PAI/ZnO	0	93.65 (0.40)	90.08 (2.02)
3	ST1-PAI/ZnO	1.0	93.15 (1.03)	92.09 (0.12)
4	ST1.5-PAI/ZnO	1.5	92.65 (0.49)	84.66 (0.98)
5	ST2-PAI/ZnO	2.0	91.57 (0.10)	90.49 (0.53)
6	ST3-PAI/ZnO	3.0	91.16 (0.66)	89.64 (1.23)
7	ST4-PAI/ZnO	4.0	89.28 (0.23)	87.43 (0.73)
8	ST5-PAI/ZnO	5.0	87.82 (1.22)	90.89 (0.84)
9	ST6-PAI/ZnO	6.0	87.14 (1.20)	84.35 (1.25)
10	ST7-PAI/ZnO	7.0	84.75 (3.10)	86.98 (0.99)
11	ST8-PAI/ZnO	8.0	86.24 (2.23)	87.05 (0.89)
12	ST9-PAI/ZnO	9.0	84.84 (0.90)	85.42 (0.25)

Swelling characteristics of semi-IPN biocomposites

The swelling tendency of the prepared biocomposites was followed volumetrically by measuring their as-prepared and swollen-state diameters using a calibrated digital compass (Mitutoyo Digimatic Caliper, Series 500, resolution: 0.01 mm). The equilibrium swelling degree φ_V was determined in ref. 12 and 13:

$$\varphi_V = \frac{1}{\nu_2} = \frac{(D/D_0)^3}{\nu_2^0} \quad \text{and} \quad \nu_2^0 = \left[1 + \frac{\left((m_{ap}/m_d) - 1\right)\rho}{d_w}\right]^{-1} \tag{1}$$

where D_0 and D are the measured diameters of the samples after the preparation and equilibrium swelling, respectively. m_{ap} and m_d are the masses of semi-IPN samples of the as-prepared state and after the drying procedure, ρ is the density of the copolymer PAI gel as 1.35 g mL^{-1},[14,15] and d_w is the density of the polymerization solvent, water as 1.0 g mL^{-1}. Based on the assumption of the isotropic volumetric swelling of polymeric, ν_2^0 and ν_2 are the structural parameters representing the network character of hybrid structure, namely, the volume fraction of polymer chains as-prepared state and in the equilibrium swollen state. The gel fraction w_{gel}, that is, the conversion of monomers to crosslinked polymer was determined by $w_{gel} = [(m_0 - m_{dry})/m_0] \times 100$ using the masses of samples after the preparation state as well as the extracted and dried state. Salt-induced swelling of the semi-IPN biocomposites with various ST contents was tested in different salts: NaBr, NaCl, $NaNO_3$ and Na_2SO_4 by following the volume change of samples by abruptly changing the salt concentration between 10^{-5} M and 1.0 M. The temperature-dependent swelling testing was performed between 25 to 75 °C. During the temperature-induced swelling measurements, the diameter of the samples was measured after equilibration at one temperature, and then the samples were re-equilibrated at another temperature. pH-induced swelling was tested in the range of the 2.1–11.2 pH interval by following the volumetric volume change. Standard pH buffer solutions were prepared following the IUPAC standards and procedures.[16] The solutions in the pH 2–3 range were prepared using HCl and KH_2PO_4 salt, pH 4–7 solutions were

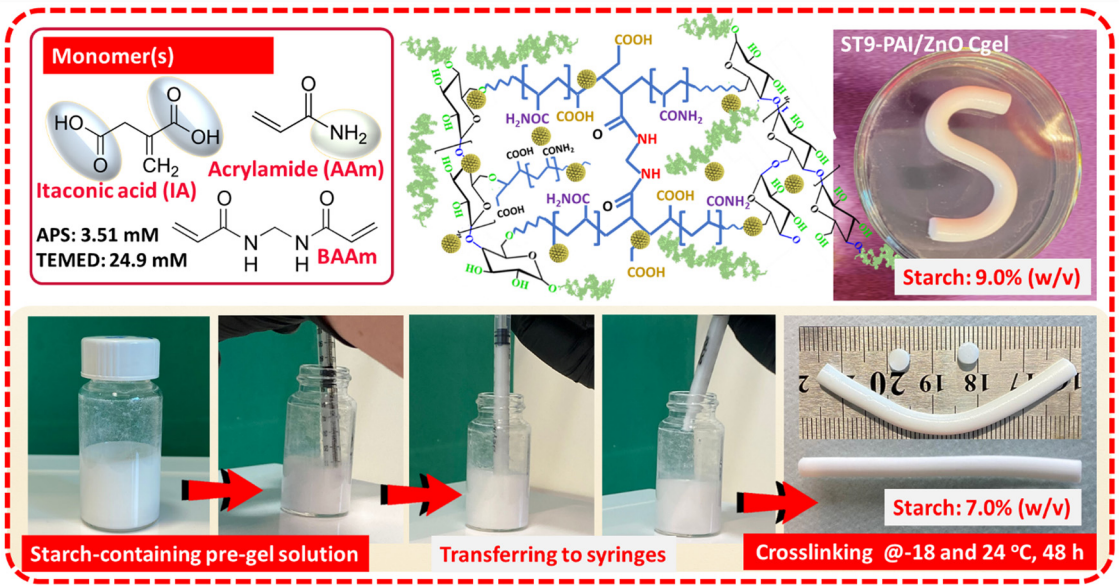

Scheme 1 Proposed mechanistic pathway for the synthesis of ST-PAI/ZnO matrix.

prepared using KH_2PO_4 and Na_2HPO_4, pH 8–10 solutions were prepared using KH_2PO_4 and $Na_3PO_4{\cdot}12H_2O$, and pH 11.2 solution was prepared using Na_2HPO_4 and $Na_3PO_4{\cdot}12H_2O$ at room temperature. For dynamic swelling/deswelling kinetics measurements in pH 2.1 and 11.2, the change in the mass of samples was followed as a function of the deswelling time in basic solution at pH 11.2 and swelling time in acidic solution at pH 2.1 to determine the water uptake $\varphi(t)$ and the relative weight swelling ratio φ_{rel} as follows:

$$\varphi(t) = \frac{m_t - m_d}{m_d} \quad \text{and} \quad \varphi_{rel} = \frac{m_t}{m_{sw}} \tag{2}$$

where m_t and m_{sw} are the masses of samples at swelling time t and equilibrium-state, respectively.

Uniaxial compression testing of semi-IPN biocomposites

The mechanical properties of semi-IPN biocomposites were characterized by uniaxial compression tests after-synthesis and after the swelling equilibrium in water. In the as-prepared case, the sample diameter/length remained constant at 4/5 mm, while the proportion of gels reaching swelling equilibrium varied. Finally, three or four samples were measured for each ST concentration and the ambient temperature was controlled at 23 °C. During the measurements, the samples were uniaxially compressed using a vertically fitted circular probe with a diameter of 40 mm. Compression was performed to 0.5 mm min^{-1} and the corresponding change in the length of the testing sample was followed using a digital comparator (IDC type Digimatic Indicator 543-262, Mitutoyo) sensitive to displacements of 10^{-3} mm. After each loading, the corresponding decrease in the height of the sample was followed as; $\Delta L = L_{in} - L$, in which L_{in} and L are the lengths of the sample before and after loading along the vertical axis, respectively. The compressive modulus, G, was determined from the nominal stress, σ, using the equation:[17]

$$\sigma = f/A_0 = G(\alpha - 1/\alpha^2) \tag{3}$$

where f is the compressive force measured after 15 s relaxation of the network chains for attaining the equilibrium. A_0 is the cross-section of the sample determined from the initial diameter $A_0 = \pi(D_0/2)^2$and α is the corresponding deformation ratio of the sample defined as the ratio of displacement ΔL to the length before the compression L_{in} along the vertical axis. After plotting the stress–strain curves, the compressive modulus was evaluated from the compressive curve in the initial strain range of 20%.

Batch adsorption experiments of semi-IPN biocomposites

Adsorption studies on methyl violet (MV) dye were performed using a batch technique using an orbital shaker at 100 rpm at ambient temperature. MV, which is widely used in textile, paint and paper dyeing, is an important industrial dye whose presence in trace amounts in water poses a serious threat to treat MV pollution in the environment. Since cationic MV dye with an amine functional group is mutagenic, the ecological impact of releasing this dye into the environment is concerning. For the adsorption of MV dye on semi-IPN biocomposites, initially weighed amounts of dry samples were immersed in 15 mL of solution containing 50 mg L^{-1} of dye. Firstly, aqueous solutions of MV were prepared by dissolving known amounts of dye in distilled water, then the dried samples were immersed under constant stirring. Using a UV-visible spectrophotometer at 577 nm, the residual concentration of MV in the solution was determined by using a calibration graph ($A = 0.01793 + 0.1162C$, $R^2 = 0.9987$). The absorption capacity of semi-IPN biocomposites at equilibrium q_e (milligrams of dye per gram of dry sample) was calculated using the following equation:

$$q_e = \frac{(C_i - C_e)V}{m} \quad \text{and adsorption } (\%) = \frac{(C_i - C_t)}{C_i} \times 100 \tag{4}$$

where C_t is the concentration of MV at time t (mg L^{-1}), C_i and C_e (mg L^{-1}) are the initial and final concentrations of MV dye, respectively, V and m are the solution volume (L) and adsorbent weight (g), respectively. Adsorption thermodynamics was investigated to get an idea of the adsorption behavior as well as to predict the spontaneous nature of the adsorption. For the adsorption process, the standard Gibbs free energy change ΔG° values were calculated using the van't Hoff equation:

$$\Delta G^\circ = -RT \ln K_c \quad (5)$$

where K_c is the thermodynamic equilibrium constant of adsorption (L g^{-1}), which can be calculated using the adsorption data, T is the absolute temperature in K, and R is the gas constant (8.314 J K^{-1} mol^{-1}).

Instrumental characterization of semi-IPN biocomposites

Fourier transform infrared (FTIR) spectra of semi-IPN biocomposites were recorded using a PerkinElmer spectrum 100 FTIR spectrometer using the attenuated total reflection (ATR). The dried samples were finely powdered before the measurements. The data were recorded at room temperature in the wavenumber range of 4000–650 cm^{-1} at a spectral resolution of 4 cm^{-1} with an average of 120 scans for each spectrum. X-ray diffraction patterns of semi-IPN samples were recorded on a Bruker D8 Advance X-ray diffractometer wide-angle XRD with CuKα radiation (λ = 1.5420 Å) operating at a voltage of 40 kV and 40 mA with a scan step time of 2° min^{-1}. Dried gel samples were powdered and the data were recorded in the 2θ range of 4–50°.

Results and discussion

The synthesis of semi-IPN biocomposites was performed by a conventional free radical polymerization process using ST, AAm, IA and ZnO as the monomers with APS as the unimolecular initiator and BAAm as the crosslinker. A facile solution technique was employed with water as the medium for the preparation of hybrid biocomposites. The use of ST for modification of PAI/ZnO was intended to study its effect on the swelling extent. Since the semi-IPN biocomposites exhibited different swelling behaviors at various pH values, their pH reversibility was investigated in aqueous solutions adjusted to pH 2.0 and 11.2. The synthesized biocomposites were taken as an adsorbent in the removal of methyl violet dye from water.

Structural characterization of starch blended ZnO-embedded biocomposites

Fig. 1 presents FTIR spectra of semi-IPN biocomposites measured in the range of 4000–650 cm^{-1}. The broad band in the FTIR spectrum of raw ST detected at 3345 cm^{-1} was due to the stretching mode of OH groups. The functional groups identified from FTIR of raw ST are presented in Table S1 in the ESI.† It was previously reported that the peak at 3300 cm^{-1} is due to

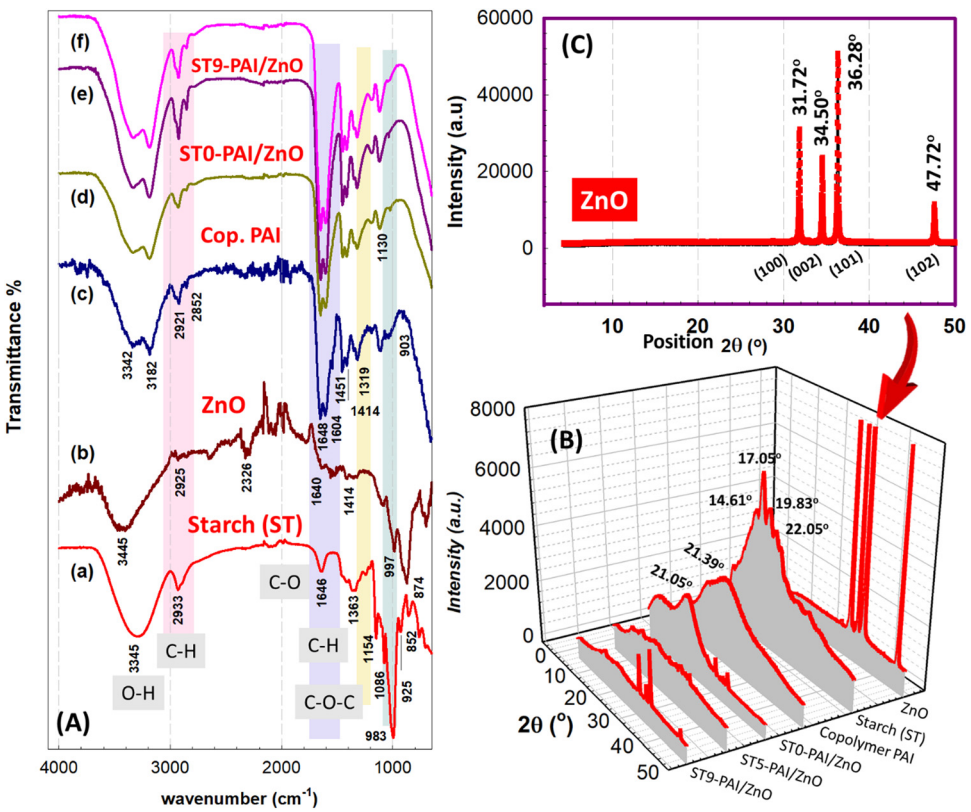

Fig. 1 (A) ATR-FTIR spectra of hybrid biocomposites: raw ST (a), ZnO (b), copolymer PAI gel (c), ST-free ST0-PAI/ZnO gel (d), ST9-PAI/ZnO gel (e) and cryogel (f) containing 9.0% (w/v) of ST in the feed. (B) and (C) XRD patterns of raw ST and copolymer and hybrid biocomposites.

the water directly bonded to OH groups of starch double helices *via* hydrogen bonds.[18–20] The absorbance peak at around 1646 cm^{-1} is assigned to the intermolecular H-bonding and C–O bending associated with the OH group, while the peaks at 1422 and 1466 cm^{-1} are assigned to the C–H symmetrical scissoring of the CH_2OH moiety. The peaks at 1246 and 1335 cm^{-1} are due to the O–H bending of the primary or secondary alcohols. The band assigned to C–O stretching at 1154 cm^{-1} was also observed around 1151 cm^{-1} in the FTIR spectra of semi-IPN biocomposites. In the raw ST, the stretching vibration of C–O was detected at 1086 cm^{-1}, while the increase in the peak intensity was observed around 1085 cm^{-1} in semi-IPN biocomposites. The bands at around 2930 cm^{-1} are assigned to C–H stretching. Previous studies have reported that the 800–1300 cm^{-1} region is sensitive to changes in the ST polymer conformation.[21,22] In more detail, the characteristic bands of near 930 cm^{-1}, 1020 cm^{-1}, 1085 cm^{-1}, and 1137 cm^{-1}, in semi-IPN biocomposites are possibly attributed to α-1,4 glycosidic bond skeleton vibration, coupled vibration of C–O and C–C, C–O–H bending vibration as well as the C–O–C stretching vibration.[21] Pozo and coworkers[18] reported that the intensity ratio of FTIR bands at 1020 and 1040 cm^{-1} is an indicator of ST crystallinity, and the short-range ordered structure of the double helices of amylopectin side chains can be observed at 925 and 852 cm^{-1}. These bands are assigned to the COH bending vibration and CH_2-related modes of the α-D-glucopyranose ring. It was reported in the study of Lu *et al.* that the absorbance at 1047 cm^{-1} is related to the crystallization region of starch, whereas the amorphous area is reflected by the absorbance of 1022 cm^{-1}.[20]

In the FTIR spectrum of ZnO, the broad band at 3445 cm^{-1} is due to the O–H stretching mode of the hydroxyl group resulting from the hygroscopic nature of ZnO. The series of peaks at 1312, 1355, 1414, 1509, 1561, and 1640 cm^{-1} in the region extending from 1300 to 1650 cm^{-1} are likely assigned to the bending modes of O–H bonds bound and the adsorbed water, respectively. Keyes and coworkers observed similar peaks in the infrared spectroscopy of polycrystalline ZnO.[23] The bands in the region of 1700–650 cm^{-1} corresponded to C═O, C–O and C–H vibrations.[24] It has been also reported that the absorption bands observed at 1700–1400 cm^{-1} arise from the OH bending of adsorbed moisture in ZnO-containing samples.[25] The absorption at 874 cm^{-1} is due to the formation of tetrahedral coordination of Zn. The band at 997 cm^{-1} is due to C–O stretching vibration, while the observed peaks at 713 cm^{-1} indicate the stretching vibrations of ZnO particles. Similarly, the presence of an absorption band at 1020–950 cm^{-1} of semi-IPN biocomposite samples is due to the vibration of Zn–O.

The FTIR spectra of copolymer PAI showed the absorption peaks for IA at 1648 cm^{-1} with C═O stretching vibration of COOH groups, and for acrylamide at 1604 cm^{-1} and at 3342 cm^{-1} originating from the secondary amines in acrylamide. It showed amide II peaks at 1529 cm^{-1} and the peaks that appeared at 1451 cm^{-1} and 1414 cm^{-1} were attributed to the symmetric stretching of COO^- groups. The absorption peak at 1319 cm^{-1} is due to the C–N vibration absorption of the amide groups in accordance with the results of Ma and coworkers for ternary hydrophilic copolymer of IA, AAm and sodium *p*-styrene sulfonate.[26] The fact that these peaks appear with increasing intensity in semi-IPN gels indicates that the interactions in the structure have increased. In the FTIR spectra of the copolymer PAI and ST-PAI/ZnO gels, the peaks that appeared at 2921 cm^{-1} and 2852 cm^{-1} corresponded to the asymmetric and symmetric stretching frequency of CH_2 groups present in acrylamide and IA in the copolymer network structure, respectively. In the spectra of semi-IPN biocomposites, the peak around 1013 cm^{-1} represents the ether linkage (C–O–C) present in the starch moiety. The results are consistent with those of starch and itaconic acid-based superabsorbent hydrogels prepared by Bora and Karak.[5] When compared with the FTIR spectrum of copolymer IA, ZnO and ST, the shifts in the characteristic bands of OH, amide and COOH and the increase in the peak intensities indicate the formation of hydrogen bonds between ZnO, ST and copolymer PAI.

Fig. 1B shows XRD patterns of ZnO and the obtained diffraction planes. The XRD pattern of ZnO exhibited sharp peaks, as shown in Fig. 1C, confirming its crystalline nature. The major diffraction peaks, which are observed between 2θ = 30° and 50°, corresponded to the hexagonal ZnO crystal-structure. The higher intensity peaks in the XRD pattern of ZnO detected at 31.72° (100), 34.50° (002), 36.28° (101), and 47.72° (102) corresponded to the (100), (002), (101), and (102) planes of hexagonal ZnO nanoparticles, respectively. These lines well matched the values reported by JCPDS (No. 36-1451).[25,27] The crystallinity of ZnO refers to a structure of wurtzite being hexagonal in shape which is the result of the penetration of the two hexagonal lattices. The crystalline nature of ZnO nanoparticles with hexagonal structure has been reported by previous studies.[28–30] In the XRD pattern of ZnO, all peaks with their diffraction angles are perfectly matched with reported peaks of pure hexagonal wurtzite structure ZnO nanoparticles. As seen in Fig. 1B, the copolymer PAI gel has an amorphous structure, showing a broad peak around 21.39°. After the addition of ZnO, the XRD pattern of ST-free ST0-PAI/ZnO gel exhibits the characteristic peak of ZnO and PAI structures, the maximum was shifted to 21.05° and additional sharp peaks were observed at 31.50°, 34.50° and 36.06° with other weak peaks at 28.50° and 30.72°. In the copolymer PAI structure, no peak was observed in this range due to its amorphous structure. As shown in Fig. 1B, the peak at 2θ lower than 30° may be attributed to the presence of ST and copolymer PAI network and the sharp peaks at 2θ from 31° to 36° are related to crystalline ZnO. A similar observation has been reported by Wang and coworkers for ZnO/carboxymethyl chitosan composites.[31] Based on this, it confirms that the presence of peaks in this range in the structure ST-free ST0-PAI/ZnO gel containing ZnO but not ST is due to ZnO particles in the structure. The XRD pattern of raw ST is a typical type B pattern shown in Fig. 1B. The characteristic diffraction peaks were observed at 2θ = 14.61°, 17.05°, 19.83°, 22.05° and 23.83° with weak diffraction peaks at 2θ = 5.06°, and 26.49°. These results are consistent with the previous report, indicating that the

packaging arrangement of type A starch is compact and the water molecules are present between each double helical structure.[18] XRD pattern of hybrid biocomposite ST9-PAI/ZnO exhibits the characteristic peaks of ST with a weak diffraction peak at 17.28°, indicating that the sample has a low crystallinity and also exhibits the characteristic peaks at 32.05°, 34.61°, 36.38° and 47.83° due to ZnO. The XRD pattern of the hybrid biocomposites showed the characteristic peaks of ST, ZnO and copolymer PAI structure indicating that all components are incorporated in the crystalline structure.

Swelling tendency of starch blended ZnO-embedded biocomposites

Network characteristics of semi-IPN biocomposites are presented in Fig. 2. After the swelling process, the experimental and theoretical ν_2^0 values were determined using eqn (1) and the results are shown in Fig. S1 in ESI.† For both ST-PAI/ZnO Hgel and Cgel samples, the volume fraction of crosslinked polymer as-prepared state values was compatible with the theoretical values at all ST concentrations and tended to increase with increasing ST in the feed. Table 1 shows the variation of the gel fraction of ST-PAI/ZnO gels with varying ST content. The gel fraction decreases from 93.1 to 84.8% with increasing ST content from 1 to 9% (w/v). By adding the redox-initiator pair to the pregel mixture containing ST, ZnO, AAm, and IA, an interpenetrated polymer network, semi-IPN, was formed by chemical crosslinking of poly(AAm-*co*-IA) and physical crosslinking of ST backbone. As ST content increases, the amount of ST entrapped in the semi-IPN matrix also increases. This result is supported by the increased polymer volume fraction after preparation-state. Since the gel fraction reflects the structural integrity of biocomposites *in vitro*, the gel fraction results confirmed that the biocomposite cryogels had relatively higher integrity compared to the hydrogels among all the synthesized samples. As a result of the increased cross-linking, less swelling is observed as the expansion flexibility of the crosslinked chains decreases. Similar results have been reported by Kundu and Banerjee for microcrystalline cellulose-based hydrogels. The experimental gel fraction followed the reverse swelling trend, and the gel with the highest gel fraction swelled the least due to the higher degree of crosslinking.[32] In the synthesis pathway, the sulfate anion radicals generated from thermally decomposed initiator APS remove hydrogen from the hydroxyl group of ST and form alkoxy-radicals on the ST backbones. This persulfate-saccharide redox-system leads to the active centers on ST backbones radically initiating the free-radicalic copolymerization of AAm and anionic comonomer IA monomers, thus forming the anionic copolymer. Then, the graft copolymer comprises a crosslinked copolymer structure since fixed amount of crosslinking agent BAAm is included in the pre-gel solution. The chemical crosslinking and electrostatic interactions were carried out between the main functional groups of ST (–OH), acrylamide (–$CONH_2$), and IA (–COOH) components of the synthesized ST-PAI/ZnO.

In Fig. 2(B), as can be seen from the optical images of the hybrid ST7-PAI/ZnO Cgel sample containing 7.0% (w/v) ST in the feed, after the synthesis period was completed and removed from the syringe, the gels were prepared in a way that they can be handled and easily worked. Various concentrations of ST 1–9% (w/v) were used to enhance the water absorption capacity of the biocomposite PAI/ZnO gels. Fig. 2(A) shows the equilibrium volume swelling ratio as a function of ST concentration in the feed. The swelling behavior of ST-PAI/ZnO hydrogels and cryogels is affected significantly by changing the ST content of the PAI/ZnO network. In both hydrogels and cryogels, the swelling followed the decreasing order of copolymer PAI > starch-free PAI/ZnO > ST-PAI/ZnO gels. By adding ZnO nanoparticles to the copolymer PAI hydrogel containing 2 mol% itaconic acid, the swelling ratio decreased from 898.1 ± 3.2 to 442.2 ± 2.7. Then, with the addition of 9% (w/v) ST to this structure, the swelling ratio further decreased to 68.3 ± 2.3. Specifically, ZnO particles act as both nanofillers and physical crosslinkers through the formation of hydrogen bonds with functional groups of the copolymer PAI matrix. Then, with the addition of ST to the PAI/ZnO structure, the swelling tended to

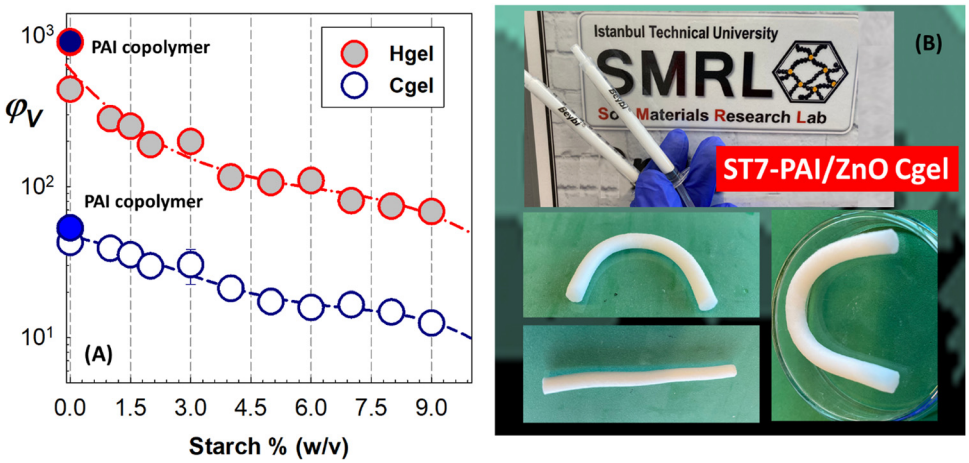

Fig. 2 (A) Equilibrium volume swelling ratio φ_V of ST-PAI/ZnO gels shown as a function of ST concentration. (B) Optical images of hybrid ST7-PAI/ZnO Cgel sample containing 7.0% (w/v) starch in the feed.

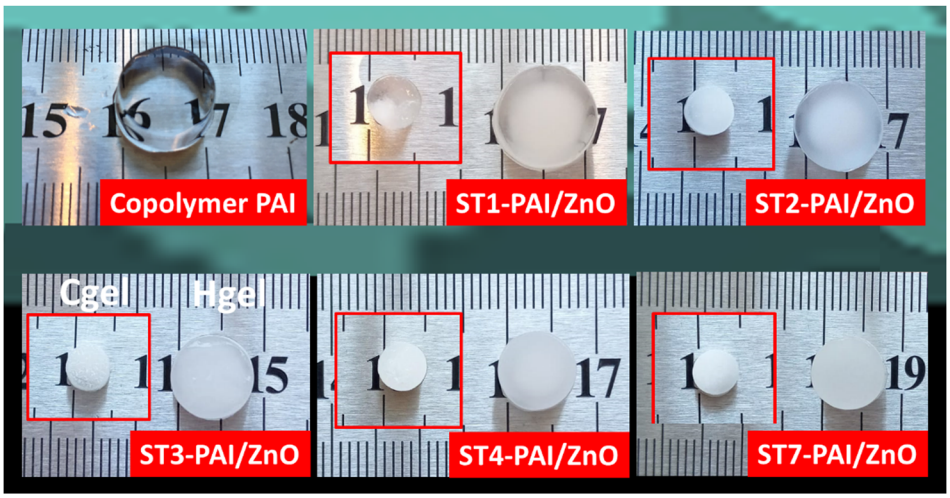

Fig. 3 Swollen state-appearances of semi-IPN biocomposites after swelling in water.

decrease continuously. As can be seen from the swollen state appearance of semi-IPN biocomposites after swelling in water, as shown in Fig. 3, as ST was added to the PAI/ZnO structure, the appearance of the samples changed from translucent to completely opaque. Intermolecular H-bonding interactions between the functional groups of ZnO and the polymer chains have been reported by various groups. The analysis results of Keshavarzi and coworkers for the effect of ZnO nanoparticles on the mechanical and rheological properties of the polylactic acid/polypropylene nanocomposites indicated that ZnO nanoparticles as filler can restrict the mobility of the polymer chains, leading to the enhancement of elasticity.[33] In their study, Li and coworkers reported that the impeded the order of the polymer chains by both steric effect and intermolecular hydrogen bonds. The incorporation of ZnO nanoparticles into chitosan increased the flexibility of the polymer chains by reducing the crystallinity of the composite membranes.[27]

Pourjavadi and coworkers reported the synthesis of magnetic Fe_3O_4@SiO_2 nanoparticle-containing starch-*graft*-poly(acrylic acid) superabsorbent nanocomposite hydrogels.[34] Their results showed that the addition of magnetic nanoparticles had a decreasing effect on the swelling of hydrogels. Adding 0.5 g of the magnetic nanoparticles to the matrix resulted in a 33% decrease in the water absorbency. A similar decrease has been reported for the swelling of the nanocomposite adsorbents prepared through free radical graft copolymerization of the AAm monomer onto starch backbones in the presence of graphene oxide nano sheets with different nano-hydroxyapatite (HAP) contents. It was shown that the addition of 5 wt% HAP resulted in a 44% decrease in water uptake of polymer.[35] Conversely, the addition of natural char nanoparticles in the matrix of starch-*g*-poly(acrylic acid-*co*-acrylamide) superabsorbent composites resulted in a two-fold increase in water absorbency in comparison with neat hydrogel.[36] It has been stated that increasing the particle radius and therefore decreasing the conformational entropy of the polymer is important in the uniform distribution of fillers in the structure. In the spatial distribution of fillers in the network, their functionality is controlled by the enthalpic effects and the particle sizes are controlled by the entropic effects. Li and coworkers have reported the synthesis of starch-*graft*-poly(acrylamide)/attapulgite superabsorbent composite.[37] Their results indicated that attapulgite content affected the swelling of composites. Compared to pure hydrogel, a 40% increase in the swelling ratio occurred with 10% attapulgite content.

Effect of starch content on semi-IPN strength and crosslinking density

The introduction of starch into the copolymer PAI/ZnO resulted in starch dose-dependent swelling-induced mechanical strength. Fig. S2 in ESI,† shows the stress–strain curves of ST-PAI/ZnO hydrogels from the uniaxial compression tests after the preparation state and after the swollen state as well as the stress–strain curves of ST-PAI/ZnO Cgels after swelling. Fig. S2(D) (ESI†) shows the finger compression of ST1-PAI/ZnO Hgel sample containing 1.0% (w/v) of ST in the feed. Fig. 4(A) compares the compressive elastic moduli of the ST-PAI/ZnO Cgel and Hgel samples after equilibrium swelling in water as a function of ST concentration. In general, increasing the amount of ST caused an increase in the elastic modulus of semi-IPN biocomposites. The compressive modulus of ST-PAI/ZnO Cgels increased from 9.35 ± 0.50 kPa to 22.28 ± 3.95 kPa as the ST content increased from 1 to 9% (w/v). The biocomposite cryogels exhibited significantly higher modulus than the hydrogels compared to a fixed amount of ST. With the addition of 7% (w/v) ST, the elastic modulus of the cryogel sample ST7-PAI/ZnO was 13.1 ± 2.4 kPa, while the modulus of hydrogel was 854.3 ± 9.2 Pa. Fig. S3 in the ESI,† shows the optical appearances of ST-PAI/ZnO hydrogel and the cryogel samples containing 1.5% and 7% (w/v) ST in the feed during uniaxial compression. The decrease observed in the elastic modulus until the addition of 1.5% (w/v) ST in Fig. 4(A) can be attributed to the interaction between ST molecules participating in the gel structure. Compared to long chains, the short chains of amylose

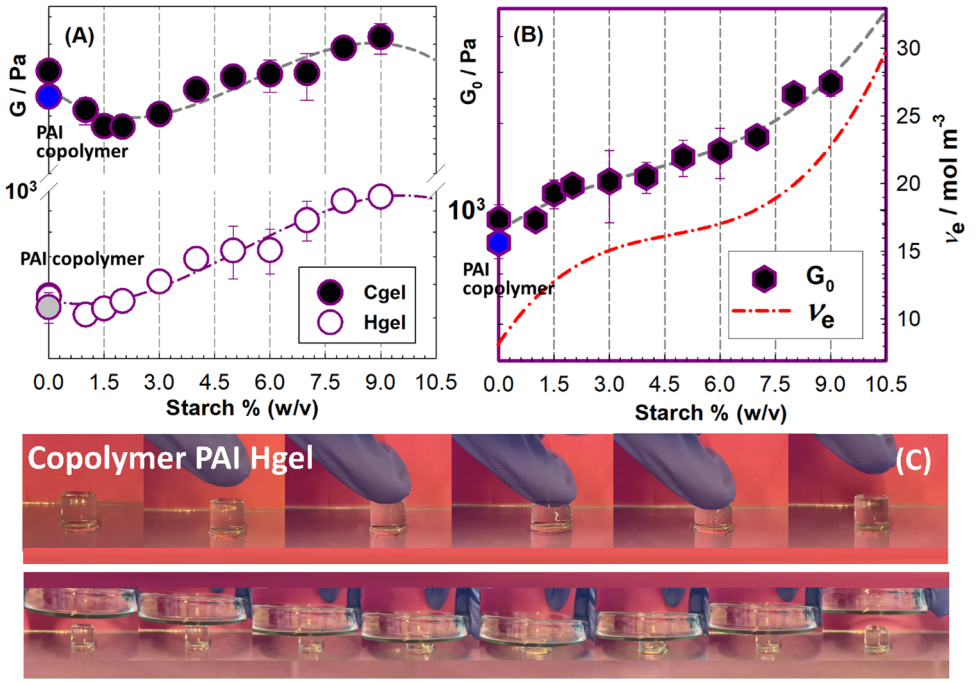

Fig. 4 (A) Comparison of compressive elastic moduli of ST-PAI/ZnO Cgel and Hgel samples after equilibrium swelling in water, (B) variation of compressive elastic moduli of ST-PAI/ZnO Hgel after preparation-state and effective crosslinking density, ν_e as a function of starch concentration and (C) optical appearances of copolymer PAI hydrogel sample during manual compression.

easily interact with amylopectin chains, largely inhibiting the swelling effect of the ST backbone. Jia and coworkers stated that the changes that ST granules undergo during the swelling process are important factors in predicting their functional properties. By breaking the hydrogen bonds between and within the ST starch chains, water molecules combine with the free hydroxyl groups in the glucan chain, causing the starch granule to swell. At the same time, amylose molecules are leached from the swollen starch granules, causing a significant increase in the viscosity.[38]

Variation of the compressive elastic moduli of ST-PAI/ZnO Hgel after the preparation state as a function of ST concentration is presented in Fig. 4(B). As can be seen from the images during manual compression, shown in Fig. 4(C), the copolymer PAI hydrogels, which had a completely transparent appearance, were quite weak and the elastic modulus in the post-synthesis state was around 770.2 ± 8.8 Pa. With the addition of ST, there was a regular increase in the elastic modulus of hydrogels after the synthesis. which might be attributed to an increase in the crosslinking density. The strong hydrophilic nature of the copolymer PAI with $-CONH_2$ groups of AAm, and –COOH groups of IA favors the formation of hydrogen bonds with –OH groups attached to the primary polymeric chain of ST, which leads to the decrease of water adsorption. A 3.6-fold increase in the elastic modulus values was observed with the addition of 9% (w/v) ST to the structure. The elasticity of the copolymer PAI network was improved by incorporating ZnO particles as well as by entangling PAI chains with ST backbones. It was previously reported that the role of nanoparticles as fillers became evident after the addition of a certain amount of ZnO nanoparticles. ZnO as fillers restricts the mobility of the polymer chain, which can lead to increased flexibility. In this study, the increased flexibility of nanocomposites loaded with 5 wt% ZnO was associated with the flexibility of the physical network of nanoparticles. It may correspond to the structural elasticity resulting from the interconnection of dispersed nanoparticles.[33] Macias-Rodriguez and Velikov investigated the reinforcement effect of starch particles for thixotropic materials such as lipid gels.[39] To explain the mechanical contribution of rigid polydisperse starch particles to lipid crystal networks, the elastic moduli and yield stresses were measured as a function of the volume fraction of embedded particles. The elastic modulus of starch-filled lipid gels increases with time, as the particle volume fraction increases, the composites gradually harden, the modulus and yield stress increase, and become brittle.[39] For the present gel system, increasing the amount of ST increased the rigidity of the semi-IPNs due to the formation of hydrogen bonds and physical entanglements between polymer chains. Non-covalent crosslinking facilitates energy dissipation, resulting in high compressive modulus and mechanical stability. Therefore, from the as-prepared state mechanical measurements, the effective crosslinking density, ν_e of the biocomposite hydrogels indicating the mole fraction of elastically active chains in the semi-IPN structure was calculated as a function of starch concentration using the elastic modulus G_0 and ν_2^0 values in the following equation:

$$\nu_e = G_0/\beta RT\nu_2^0 \quad (6)$$

To the experimental data presented in Fig. 5(B), the third-order polynomial gave the best fit to the dependence of the experimental results on the amount of starch as:

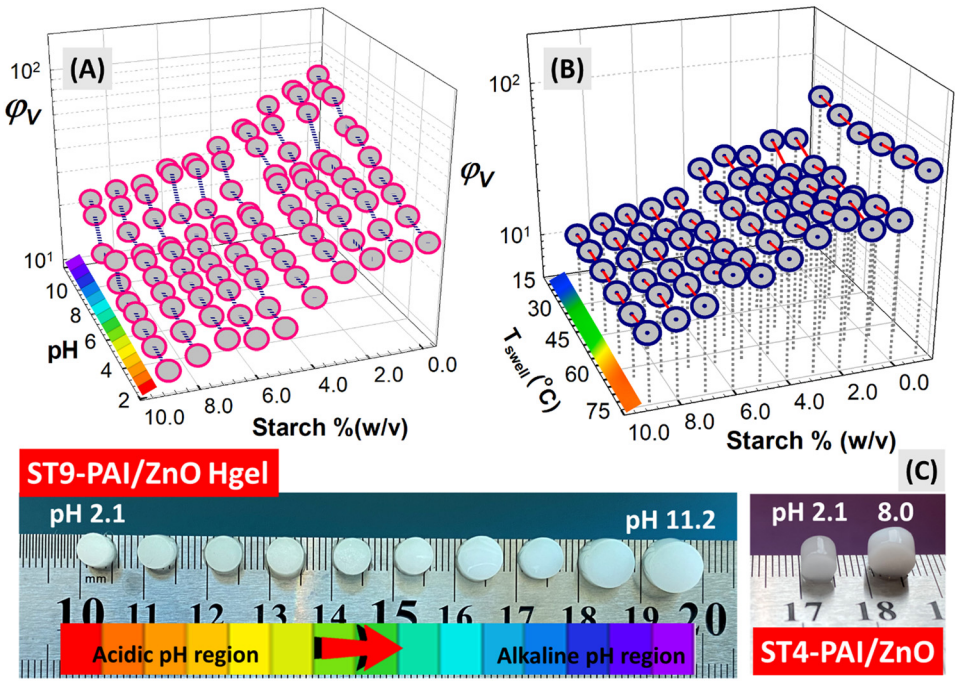

Fig. 5 pH-Sensitive (A) and temperature-induced (B) swelling results in order of increasing pH and swelling temperature as well as starch content in the feed for ST-PAI/ZnO Cgels. (C) Optical appearances of the hydrogel samples containing 4.0 and 9.0% (w/v) starch after swelling in the pH buffer solutions.

$$\nu_e = 2.890 + 0.117\ (\text{starch}\%) - 0.019\ (\text{starch}\%)^2 + 1.547 \times 10^{-3}\ (\text{starch}\%)^3 \quad (7)$$

This polynomial allows the change in effective crosslink density to be determined without synthesis when the desired amount of starch is added to the PAI/ZnO structure containing AAm/IA at a mol ratio of 98/2. The effective crosslink density of semi-IPN Hgels presented as a dashed red curve (R^2 = 0.9936) was shown to be proportional to the amount of starch used in the synthesis. This indicated that increasing the starch content allowed for greater interaction between ST and PAI/ZnO chains to occur. Therefore, the mechanical strength of the semi-IPN bicomposite depends on its microstructure. A higher degree of crosslinking improved the mechanical properties of the porous material prepared under cryoconditions. Since the ST chains in a semi-IPN biocomposite structure would disperse energy, it helps transfer the applied stress through physical entanglement, effectively dissipating local stress. In this way, it improves the mechanical strength of semi-IPNs and increases the compressibility. The higher crosslinking density of the hydrogel indicates a decrease in the free volumes as well as the mobility of the polymer chains between the network, thus indicating a decrease in the swelling ratio.[39] The results were similar to previous findings reported by An and coworkers, with the study concluding that the low swelling power of wheat starch was beneficial in increasing the elasticity of the gluten-based network.[40]

Fig. S4 in ESI,† presents the optical appearances of the ST7-PAI/ZnO Cgel sample containing 7% (w/v) in the feed during uniaxial compression. The presence of ST and ZnO particles in its structure, as well as the formation of a porous structure as a result of polymerization under cryoconditions, have made biocomposite cryogels resistant to compressive stress, which is important in articular cartilage applications. Moreover, since this is the main criterion that determines the suitability of hydrogels in bone tissue engineering applications, the focus has been on improving the mechanical properties of starch-based gels using various strategies. In their work, Sringam and coworkers improved the mechanical properties of starch-based hydrogels using a double network strategy.[41] The compressive properties of single network ST hydrogels prepared using glutaraldehyde as a crosslinker were affected by both crosslinker content and crosslinking time. The presence of a secondary network in the double network hydrogel formed using poly(vinyl alcohol) and borax as the secondary polymer and crosslinker, respectively, increased the polymer chain entanglement and crosslink density by reducing the chain freedom compared to the single network hydrogel. Since the compressive modulus of double network hydrogels varies between 25 and 35 kPa, the results compatible with the compressive modulus of articular cartilage in the superficial region 20–1160 kPa were obtained. In the present system, the compression modulus of ST9-PAI/ZnO cryogel samples prepared under cryoconditions in the presence of 9% (w/v) ST is 22.28 ± 3.95 kPa. In another strategy, oxidized ST-based gels were synthesized by both "internal crosslinking" followed by "surface crosslinking reaction". In this sequential crosslinking method, itaconic acid-based core superabsorbent polymer composites were prepared by incorporating various proportions of oxidized ST *via* aqueous solution copolymerization using APS

as the initiator and 1,6-hexanediol diacrylate as the internal crosslinker.[42] Surface crosslinking was then carried out using various surface crosslinkers with epoxide groups at both ends to produce surface-crosslinked superabsorbent polymer composites with improved gel strength. The increase in the elastic modulus was attributed to the increase in hydrogen bonds with increasing amount of ST, while the boundary between ST and polymer network was strengthened due to additional crosslinking. The contrasting trend between the swelling and elasticity in the presence of polysaccharide was reported by Martínez-Ruvalcaba and coworkers for hybrid acrylamide/chitosan hydrogels synthesized in 1% (w/w) IA solution.[43] With the addition of chitosan, the swelling capacity of hydrogels decreased and Young's modulus increased, which can be explained by the presence of ionizable groups in both chitosan and IA units.

pH-Induced swelling of starch-blended ZnO-embedded biocomposites

Fig. 5 shows the influence of the solution pH (2.1–11.2) and swelling temperature on the water absorption capacity of the prepared ST blended ZnO-embedded biocomposite cryogels as a function of ST content in the feed. For biocomposite hydrogels, pH-sensitive swelling results were presented in Fig. S5 in the ESI,† in order of increasing pH as well as ST content in the feed. The equilibrium swelling ratio of ST-PAI/ZnO gels strongly depends on pH; as the pH increased, there was a gradual increase in the equilibrium swelling at two different pH values. The first and second dissociation constants of itaconic acid are pK_{a1} = 3.85 and pK_{a2} = 5.45,[44] respectively. When pH < 4.0, most of the $-COO^-$ groups are protonated and excessive H^+ ions in the external medium suppress the ionization of carboxyl groups of ST-PAI/ZnO gels, and consequently, the flexibility of the chain is rather low. The conversion of $-COO^-$ anion to –COOH may limit the swelling and therefore reduce the swelling. Quintanilla de Stéfano and coworkers studied the pH-sensitive swelling of ST-based hydrogels synthesized by the copolymerization of acrylic acid and acrylate comonomers onto the ST backbone.[45] The hydrophilic agents 2-hydroxy ethyl methacrylate, and AAm, as well as the hydrophobic butyl-methacrylate, were utilized as comonomers. While the hydrophobic/hydrophilic character of the monomers affected the swelling properties, all hydrogel formulations were sensitive to the pH of the liquid medium, and the swelling capacity reached a maximum value close to neutral or physiological pH. A similar swelling tendency was also reported by Soto and coworkers for IA grafted onto corn starch hydrogels as metal remover.[46] It was shown that the introduction of the carboxyl and carbonyl groups promoted starch hydration and swelling. Maximum water uptake at low pH values is reported to be due to increased protonation of lower carboxylic groups, and uptake is higher as pH increases above pK_a.

As pH increases beyond 4.7, the ionization of carboxyl group units of semi-IPNs causes a gradual increase in the swelling ratio due to increased ion swelling pressure. The chain relaxation resulting from the electrostatic repulsion between the carboxylate groups within the semi-IPN matrix positively affects the overall swelling. As shown in Fig. 5, the maximum swelling ratio is observed at pH 9.8; this is due to the complete dissociation of the carboxyl groups at this pH value. However, with a further increase in the pH, a slight decrease in the ion swelling pressure begins or no change is observed because the increase in the ionic strength of the swelling medium caused a decrease in the ion osmotic swelling pressure. As shown in Fig. 5, the overall swelling values decreased with increasing ST concentration. As a result of a compact distribution of H-bonds, called the cooperative effect, increased H-bonds between the carboxyl groups of IA and OH groups of ST backbone, carbonyl or amide groups of PAAm act as physical cross-links and reduce the gel swelling. However, despite the decrease in swelling capacity, the increasing amount of ST did not cause a change in the pH-induced swelling character. As can be seen from the optical appearance of the hydrogel samples containing the maximum amount of 9% (w/v) ST after swelling in pH buffer solutions, the biocomposites had obvious pH-sensitive swelling. When the pH value was increased from 4.7 to 8.0, the swelling ratio of the biocomposite sample increased by 37.3%, while when the pH was increased to 11.2, the sample showed a strong pH response with an increase of 88.8%.

Fig. 5(B) shows the effect of swelling temperature and ST amount on the temperature-induced swelling of ST-PAI/ZnO Cgels. While a decrease in the swelling ratio of semi-IPN biocomposites was observed with increasing temperature, a slight increase in swelling was observed above 60 °C. This can be attributed to the fact that the polymer chains do not tend to expand as a result of the weakening of the interaction between the water molecules and the copolymer functional groups at low-swelling temperatures. Recently, a similar temperature-dependent increase was reported for the temperature-dependent swelling of *N*,*N*′-dimethylacrylamide/acrylic acid amphiphilic hydrogels.[47] The authors stated that high temperature caused the swelling ratio to increase, and when the temperature increased from 25 °C to 80 °C, the swelling ratio doubled. For the present semi-IPNs, when compared according to the ST content, the swelling decreased significantly with increasing ST concentration, as observed in the water swelling experiments at room temperature. Similar results were reported by Sha and Adachi for the temperature-dependent swelling pressure of tapioca starch gels investigated at a temperature range of 25–60 °C.[48] The swelling was observed to increase from 1 to 3 MPa with a temperature increase from 25 to 50 °C. The fact that the enthalpy change estimated from the swelling pressures in this temperature range was 29.9 kJ mol^{-1} showed that the swelling was endothermic. However, the observed decrease in the swelling pressure at 60 °C was attributed to the gelatinization of tapioca starch.[48] In addition to temperature, the effect of relatively small amounts of polysaccharides such as glucose, sucrose and galactose on the mechanical and optical properties of thermo-responsive gels has been reported by Drozdov and Christiansen using a simplified mean-field.[49] The point is that temperature-sensitive gels have the ability to recognize host molecules, making them suitable for applications as chemical and biochemical sensors. The results showed that the elastic modulus increases strongly at temperatures

above the critical temperature, and this increase is due to the accumulation of hydrophobic segments into the clusters that act as physical connections between the chains in the network.

pH-Triggered swelling kinetics of starch-blended ZnO-embedded biocomposites

Since semi-IPN biocomposites gradually showed volume change in response to the pH of the external medium, pH-triggered swelling kinetics were analyzed under pH conditions ranging from 2.1 to 11.2. Water absorption of semi-IPN biocomposites was monitored gravimetrically as a function of time. Fig. 6 shows the relative weight swelling ratio of ST-PAI/ZnO gels with different ST contents as a function of the shrinking time at pH 2.1 and swelling time in the solution of pH 11.2. Optical appearances of ST-PAI/ZnO hydrogel samples containing 1.0, 3.0 and 5.0% (w/v) ST after swelling in pH buffer solutions were presented for comparison. As seen in Fig. 6, semi-IPN ST-PAI/ZnO hydrogels and cryogels exhibited different swelling rates depending on the degree of ionization of the carboxylic acid groups of IA units when immersed in the solution. Semi-IPN biocomposite cryogels tended to swell and shrink faster compared to biocomposite hydrogels, whereas the swelling and shrinkage occurred more slowly in the hydrogels. The water absorbency of biocomposite cryogels increased sharply at the beginning of the swelling process, after which no sharp change in the swelling was observed until the equilibrium was reached, although slower swelling rates were observed in the biocomposite hydrogels. In addition, the swelling ratio decreased with increasing ST content for both hydrogels and cryogels. The ST7-PAI/ZnO C gel sample containing 7% (w/v) ST absorbed about 74% water within 50 min, whereas the ST7-PAI/ZnO Hgel sample absorbed only about 46%, within the same time frame. The electrostatic repulsion between the ionized groups that were formed as a result of the conversion of the carboxylic groups of IA into the ionized form $-COO^-$ in the pH 11.2 environment causes the semi-IPN biocomposites to swell. However, by immersing the gels in pH 2 buffer solution, the electrostatic repulsion is eliminated, and the biocomposites tend to shrink due to the formation of the hydrophobic interactions with the formation of hydrogen bonds between the non-ionized carboxylic acid groups of IA, the hydroxyl groups of ST and the amide groups of AAm. It was observed that the semi-IPN biocomposite cryogels shrank faster than that of hydrogels. While the ST7-PAI/ZnO Cgel sample released 49% of the adsorbed water within 50 min, the ST7-PAI/ZnO Hgel sample could only release 39% in this period.

Fig. 7 shows $\ln \varphi(t)/\varphi_W$ *versus* $\ln t$ curves of semi-IPN ST-PAI/ZnO C gels with different ST content in pH 11.2 solution. The results for semi-IPN hydrogels are presented in Fig. S6 in ESI.† To analyze the effect of ST content on the water diffusion behavior of semi-IPN biocomposites, the following time-dependent power law equation, eqn (8), was utilized for the initial 60% of the swelling in the solution of pH 11.2:[50]

$$\ln \frac{\varphi(t)}{\varphi_W} = \ln k + n \ln t \quad (8)$$

where $\varphi(t)$ and φ_W are the water absorbencies at time t (min) and at equilibrium, k is the structural constant of semi-IPN, and n is a diffusional exponent which is calculated from the intercept and slope of the curves given in Fig. 7(A), respectively.

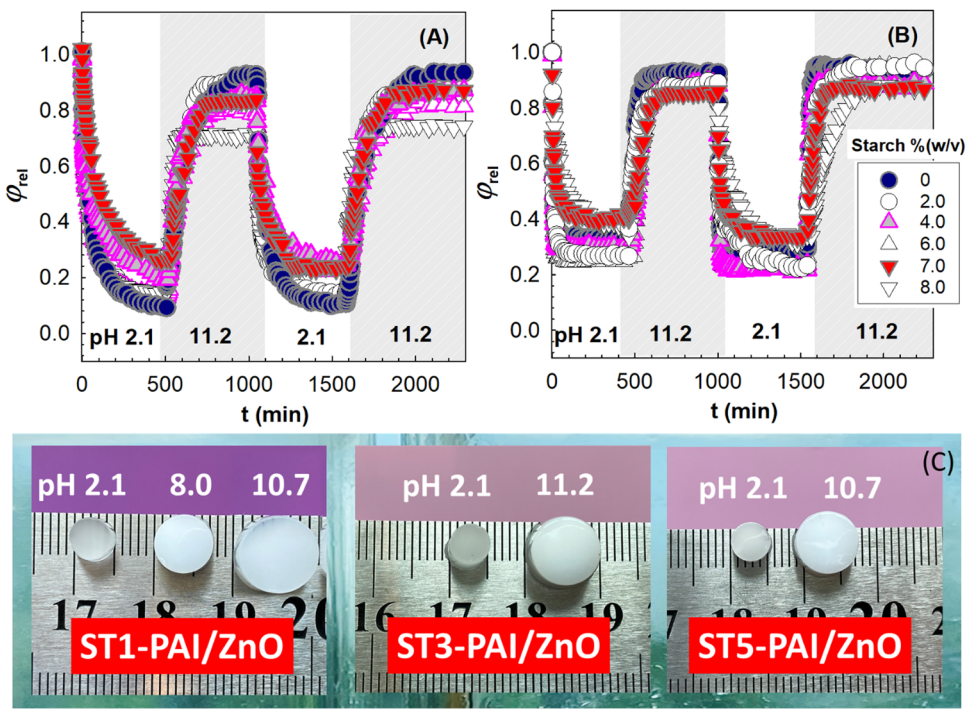

Fig. 6 Relative weight swelling ratio φ_{rel} of ST-PAI/ZnO Hgels (A) and Cgels (B) with different ST content shown as a function of the shrinking time in pH 2.1 and swelling time in pH 11.2 solution. (C) Optical appearances of ST-PAI/ZnO hydrogel samples containing 1.0, 3.0, and 5.0% (w/v) starch after swelling in pH buffer solutions.

While the calculated n values ranged between 0.2083–0.7305 for semi-IPN cryogels, however, for semi-IPN hydrogels, they were above 0.5 at all ST concentrations and ranged from 0.5085–0.6196. For semi-IPN hydrogels, n values greater than 0.45 are affected by both the diffusion of water and the relaxation behavior of the semi-IPN structure and are in accordance with the non-Fickian diffusion type at all ST concentrations. For semi-IPN cryogels, n values at low ST concentrations are much smaller than 0.45, the release is diffusion-controlled and conforms to the Fickian diffusion type. However, the increase in the n value at high ST concentration showed that the swelling occurred by a non-Fickian diffusion mechanism. Based on the short-time approximation of Fick's law, the water fraction $\varphi(t)/\varphi_W$ is directly proportional to $t^{1/2}$ and the early-stage diffusion coefficient of water D_E can be calculated using the following square root time-dependent equation:[51]

$$\frac{\varphi(t)}{\varphi_W} = 4\left[\frac{D_E t}{\pi L^2}\right]^{1/2} \quad (9)$$

where L is the size of the sample. Using the slope of the initial linear part of the water fraction $\varphi(t)/\varphi_W$ against the $t^{1/2}$ plot given in Fig. 7(B), the early-time diffusion coefficients of water D_E were determined and compared in Table 2. For semi-IPN biocomposite cryogels, D_E values were in the range of 2.0783 and 5.5696×10^{-7} cm^2 s^{-1}, while for biocomposite hydrogels, the values were changed between $1.9549–5.2329 \times 10^{-7}$ cm^2 s^{-1}. The calculated diffusion coefficients increased proportionally with the ST concentration, and this behavior confirmed that the increase in ST concentration in the semi-IPN structure favors the swelling in the acidic environment and increases the swelling rate. The calculated diffusion coefficients increased in proportion to ST concentration, confirming that ST in the semi-IPN structure increased the rate of swelling in the acidic environment. When the diffusion coefficient values are compared, the high diffusion coefficients in Table 2 show that the diffusion of water is greater with the presence of ST. Higher diffusion coefficients with increasing ST concentration indicate faster transport of water into the semi-IPN structure. This was due to the increased osmotic pressure of the semi-IPNs that water had to overcome during the swelling process. The increasing osmotic pressure with increasing ST amount is responsible for the deviation of the transport mechanism from Fickian behavior.

Since the curves of semi-IPNs deviated from linearity for all ST concentrations, it was predicted that the swelling mechanism would better adapt to second-order kinetics over longer swelling times. Based on Schott's pseudo-second-order swelling kinetics model, the average swelling rate $t/\varphi(t)$ is related to the swelling time as:[52]

$$\frac{t}{\varphi(t)} = \frac{1}{k_s \varphi_W^2} + \frac{t}{\varphi_W} \quad (10)$$

where k_s is the second-order swelling rate constant. Fig. 8 shows the variation of average swelling rate $t/\varphi(t)$ *versus* swelling time t curves of semi-IPN biocomposites with different ST content. The obtained straight lines with high correlation coefficients for both semi-IPN biocomposite cryogels and hydrogels confirmed that the swelling of semi-IPNs was second-order. The initial swelling rate is related to the relaxation rate of network chains and ST backbones in the semi-IPN structures. The ionization of the carboxylate groups, which begins at pH > 4.7, increases at a higher pH solution and the electrostatic repulsion caused by the increase in carboxylate groups causes the biocomposite network to relax. Since the

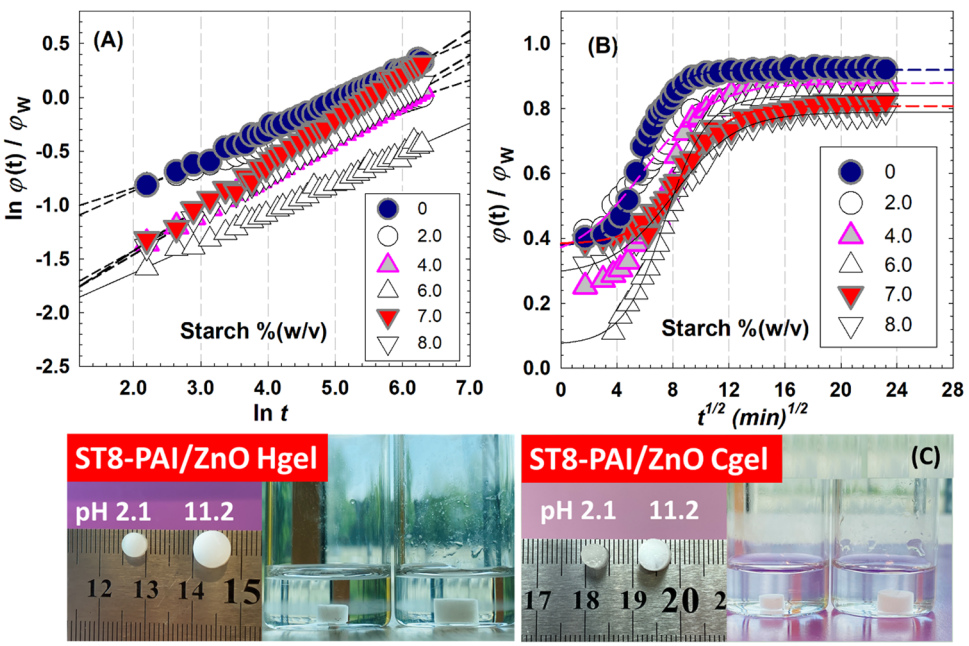

Fig. 7 (A) Plot of ln $\varphi(t)/\varphi_W$ *versus* ln t, and (B) water fraction $\varphi(t)/\varphi_W$ *versus* $t^{1/2}$ curves of semi-IPN ST-PAI/ZnO Cgels with different ST content in pH 11.2 solution. (C) Optical appearances of ST8-PAI/ZnO Hgel and Cgel samples containing 8.0% (w/v) starch after swelling in buffer solutions of pH 2.1 and 11.2.

Table 2 Kinetic exponent n, diffusion constant k, early-time diffusion coefficient of water D_E and swelling rate constant k_s for ST-PAI/ZnO Cgels and Hgels with different ST contents from the swelling in pH 11.2 solution

	ST-PAI/ZnO Cgels				ST-PAI/ZnO Hgels			
Starch (w/v)%	n	k	$D_E \times 10^{-7}$ (cm^2 s^{-1})	$k_s \times 10^{-3}$	n	k	$D_E \times 10^{-7}$ (cm^2 s^{-1})	$k_s \times 10^{-3}$
0	0.2083	0.2972	2.0783	0.2892	0.5085	0.0580	1.9549	0.3320
2.0	0.2842	0.2384	2.8319	0.7413	0.5178	0.0507	2.1135	0.7106
4.0	0.3514	0.1279	3.3233	1.0917	0.5210	0.0488	2.5563	0.8577
6.0	0.3789	0.1101	3.4361	1.1137	0.5368	0.0473	3.4073	0.8991
7.0	0.4018	0.1042	4.6799	3.1011	0.5503	0.0469	4.1172	1.1497
8.0	0.7305	0.0215	5.5696	3.4687	0.6196	0.0428	5.2329	4.4235

water molecules will penetrate the semi-IPN structure more easily as a result of rapid relaxation, the initial swelling rate can be increased.

Fig. 9 shows the swelling of ST-PAI/ZnO hydrogels at various ST contents in the presence of different salts: NaBr, NaCl, $NaNO_3$ and Na_2SO_4. Exposure of semi-IPN biocomposites to salt solutions significantly changed the degree of swelling depending on the ST content. The results for semi-IPN hydrogels are presented in Fig. S7 in ESI.† The anions reduced the swelling degree of semi-IPN biocomposites and the solubility of starch within the network. Fig. S8 in ESI,† shows the optical appearances of the ST4-PAI/ZnO Hgel sample containing 4.0% (w/v) starch after swelling in NaBr solutions of different ionic strength. The mechanical stability of the sample after swelling in 1.0 M of NaBr solution was presented. The ability to reduce the degree of swelling and solubility of ST was $Br^- > Cl^- > NO_3^- > SO_4^{2-}$ for anions and this order was consistent with the Hofmeister series.[9,10] In contrast to the structure-breaking ions, the structure-making ion; cosmotropic SO_4^{2-} anion led to a gradual decrease in the swelling at most with increasing Na_2SO_4 salt concentration. The water losses increased with increasing anion valence, as larger anions promoted shrinkage. Zhang and coworkers reported the effect of salt concentration on swelling power, and saltiness perception of waxy, normal and high amylose maize starch.[53] In all the starch samples, the swelling power decreased with increasing salt concentration which prevented the swelling and gelatinization of starch granules. The waxy starch showed the highest value, while the high amylose starch showed the least swelling power. Wang and coworkers reported similar results for the maize starch and waxy maize starch. The swelling of starch granules decreased in the order of $SCN^- > I^- > NO_3^- > Br^- > Cl^- > SO_4^{2-}$ for anions.[54] It was reported that the starch mixed with the structure-making; salting-out ions, such as SO_4^{2-} and F^- had lower swelling power and solubility as these ions may provide a protective effect on the starch and could inhibit the water absorption of starch granules. However, the structure-breaking ions or salting-in ions such as I^-, Br^-, NO_3^- and SCN^- had higher swelling power and solubility.

Adsorption studies of semi-IPN biocomposites

The adsorption capacities and removal rate toward MV dye of the adsorbents with different ST contents are depicted in Fig. 10. The adsorption sharply increased with agitation time for all adsorbents and then gradually remained after 30 min. The increase in the contact time provided a better opportunity for the interaction between semi-IPNs and MV molecules. As the contact time increases, the adsorption rate decreases as the active sites on the adsorbent surface become saturated, and the most suitable time for MV dye adsorption with an initial concentration of 10 mg L^{-1} is around 30 min. Various kinetic models including pseudo-first-order (PFO),

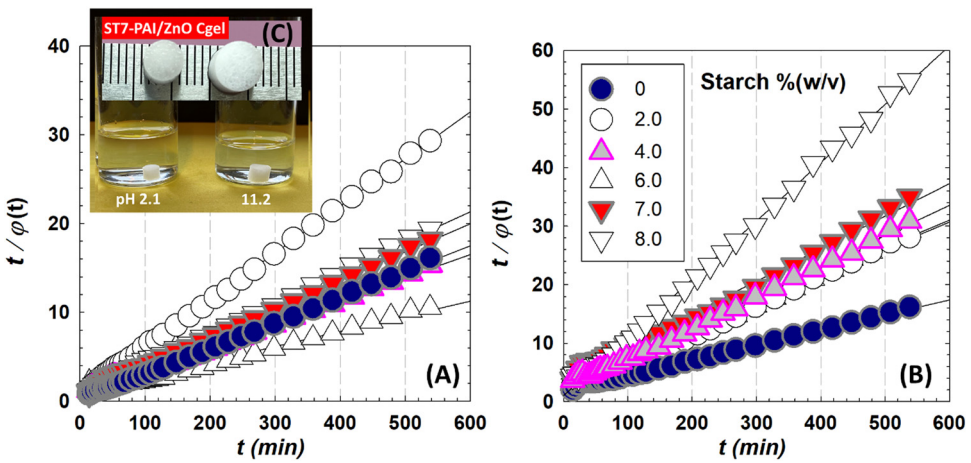

Fig. 8 (A) Variation of average swelling rate $t/\varphi(t)$ *versus* swelling time t curves of semi-IPN ST-PAI/ZnO Cgels (A) and Hgels (B) with different ST content in pH 11.2 solution. (C) Optical appearances of ST7-PAI/ZnO Cgel sample containing 7.0% (w/v) starch after swelling in buffer solutions of pH 2.1 and 11.2.

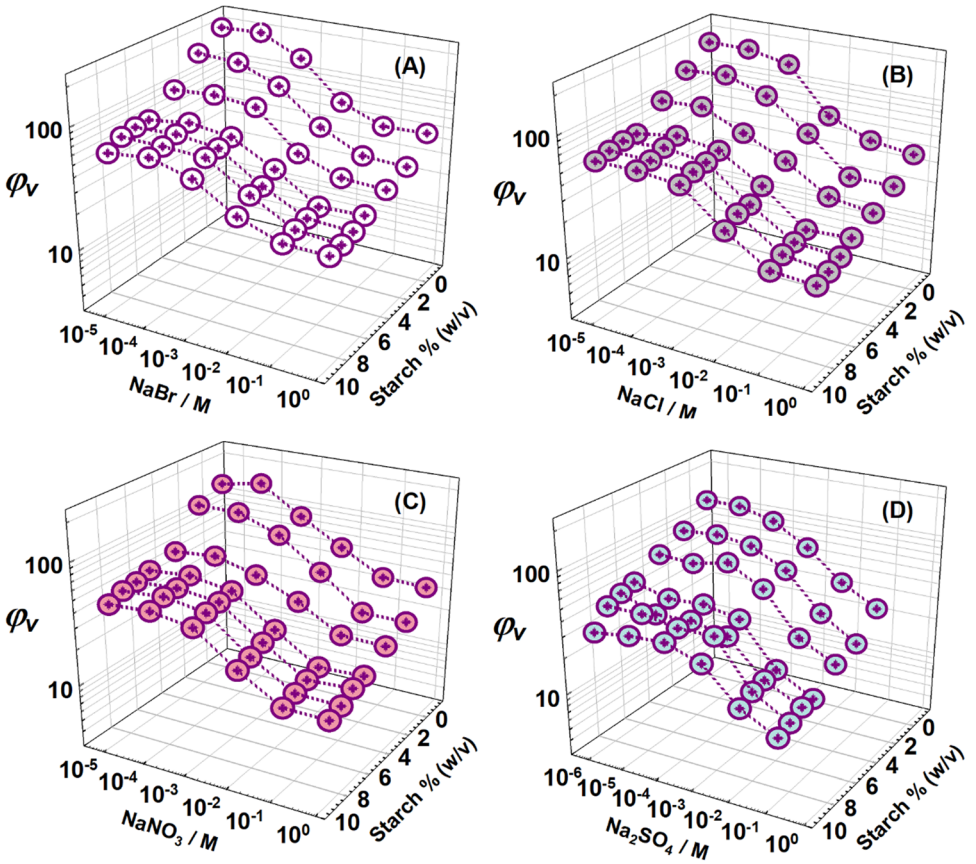

Fig. 9 Swelling of ST-PAI/ZnO Hgels with various ST content in the presence of different salts: NaBr (A), NaCl (B), $NaNO_3$ (C) and Na_2SO_4 (D).

pseudo-second-order (PSO), Elovich, and intraparticle diffusion models were used to show the most suitable model for the experimental kinetic data. These kinetic models are expressed as,

$$\ln(q_e - q_t) = \ln q_{e1} - k_1 t \quad (11a)$$

$$\frac{t}{q_t} = \frac{t}{q_{e2}} + \frac{1}{k_2 q_{e2}^2} \quad (11b)$$

$$q_t = \frac{1}{\beta}\ln t + \frac{1}{\beta}\ln(\alpha\beta) \quad (11c)$$

$$q_t = k_{diff} t^{1/2} + C \quad (11d)$$

where q_{e1} is the theoretical equilibrium adsorption and k_1 is the rate constant of the PFO kinetic model (min^{-1}). The values k_1 and q_{e1} were determined from the slope and the intercept of the plot of $\ln(q_e - q_t)$ against t in Fig. 11(A). However, straight lines could not be obtained from the PFO kinetic model and the correlation coefficients (Table 3) were high and the calculated q_{e1} values (Table S3, ESI†) were not compatible with the experimental values. The results for the semi-IPN biocomposite hydrogels are presented in Table S2 in ESI.† In eqn (11b), q_{e2} and k_2 (g mg^{-1} min^{-1}) are the theoretical equilibrium adsorption and PSO rate constant, respectively. Based on this model which depends on the amount and quantity of dye adsorbed on the adsorbent surface, the slope and the intercept of the plot of t/q_t *vs.* t in Fig. 11(B) gives q_{e2} and k_2 values, as presented in Table 3 and Table S3 in ESI.† As the calculated q_{e2} values by PSO kinetic model in the MV solutions in Table S3 (ESI†) were very close to the experimental values, as well as the R^2 of the PSO kinetic model was much higher than that of the PFO kinetic model, the adsorption process of MV by semi-IPN biocomposites followed the PSO kinetic model. Junlapong *et al.* proved the removal of methylene blue from aqueous media with a biodegradable cassava starch-based adsorbent following the Freundlich and pseudo-second-order kinetic model.[55] In another research, Arayaphan *et al.* reported the sorption of methylene blue onto cassava starch-based double network hydrogel was best described by this model and controlled by chemisorption *via* hydrogen bonding and electrostatic interactions.[56] Similarly, Bakhshi and Darvishi investigated the uptake of crystal violet and methylene blue by starch-*g*-poly(sodium methacrylate) hydrogel composites reinforced by eggshell particles using pseudo-second-order kinetics, indicating that the chemical sorption is the rate-limiting step.[57]

The Elovich model given by eqn (11c) can be used to elucidate the chemisorption processes that follow the second-order kinetics assuming that the surface of the adsorbent is energetically heterogeneous in nature. In this model, α is the initial adsorbate adsorption rate (mg g^{-1} min^{-1}) and β is the adsorption constant (mg g^{-1} min^{-1}). From the plot of q_t *vs.* $\ln t$,

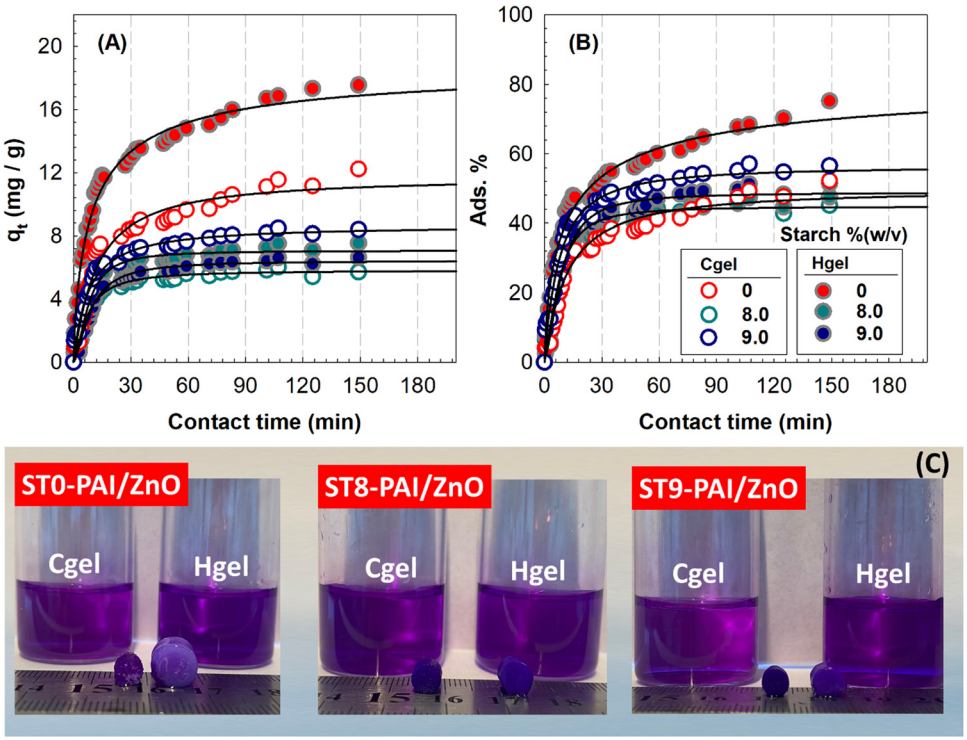

Fig. 10 Time profiles of adsorption capacity (A) and adsorption% (B) of MV dye using ST-PAI/ZnO Hgels (solid symbols) and Cgels (open symbols) prepared at different ST content as a function of contact time. Dye concentration: 10 mg L^{-1}. (C) Optical appearances of samples during adsorption of MV dye.

shown in Fig. 11(C), these constants were evaluated from the intercept and slope, respectively, and are presented in Table 3. Relatively high correlation coefficients showed that the Elovich equation is valid, that the adsorption process is governed by the chemisorption mechanism, and Elovich model can be used to describe the second-order model under the assumption that the solid surface is energetically heterogeneous. Nambiar *et al.* utilized this model to analyze the adsorption of methylene blue using starch and halloysite nanotube (HNT) composite flakes and their report confirmed that the Elovich model suggests a low initial adsorption rate and reversible adsorption and this confirms the physical interaction between MB and starch–HNT flakes.[58] In Fig. 11(D), using the linearized form of the intra-particle diffusion model, the uptake of adsorbates and the change with the square root of time $t^{1/2}$ were examined. The results showed that the intra-particle diffusion model was in accordance with the experimental data, and intra-particle diffusion was the main rate-determining step during the adsorption process.

As seen in Fig. 11(D), the adsorption process has two stages and since $k_{initial} > k_{later}$, the adsorption rate is controlled by the first stage. After this stage, in which MV molecules are adsorbed by spreading on the external surface of semi-IPN biocomposites, as the adsorption sites on the exterior surface become saturated, MV molecules diffused into the inner part of the network in the second stage. In Table 3, the rather low R^2 values with increasing ST concentration indicate a relatively poor fit to the model suggesting that interparticle diffusion is not the sole mechanism in the adsorption process. Bhattacharyya and Ray explored the kinetics of malachite green and methyl violet adsorption onto PAAm-*co*-poly(hydroxyethyl methacrylate) semi-IPN hydrogels containing 4 wt% ST and their results revealed that the intra-particle fittings show multi linearity which signifies various mechanisms for dye adsorption.[59] Similarly, Sharma *et al.* evaluated the removal of brilliant blue R-250 dye in an aqueous solution using starch/poly(alginic acid-acrylamide)nanohydrogel and their results showed that the intra-particle diffusion curve appears to be divided into the three distinctive linear regions.[60] Adsorption thermodynamics was analyzed using eqn (5) to predict the spontaneous nature of the adsorption. The fitted parameters were used in eqn (5) to calculate the standard Gibbs free energy change ΔG° of the adsorption process, and the results are exhibited in Table S4 in ESI.† The adsorption process for MV dye possesses negative ΔG° values, suggesting that the adsorption processes are spontaneous, thermodynamically favorable and ST incorporation favors the adsorption process. Taweekarn *et al.* proved that the uptake of methylene blue by starch biocryogels was spontaneous.[61] The negative ΔG° values ranged from −20 to 0 kJ mol^{-1} confirming the physical adsorption as the dominant mechanism of MB adsorption on the starch cryogels. In another report, Hosseinzadeh and Ramin showed that the adsorption of malachite green dye from aqueous solution onto starch-*graft*-poly(acrylamide)/graphene oxide/hydroxyapatite nanocomposite hydrogels was feasible and spontaneous due to negative ΔG° values at all temperatures.[35]

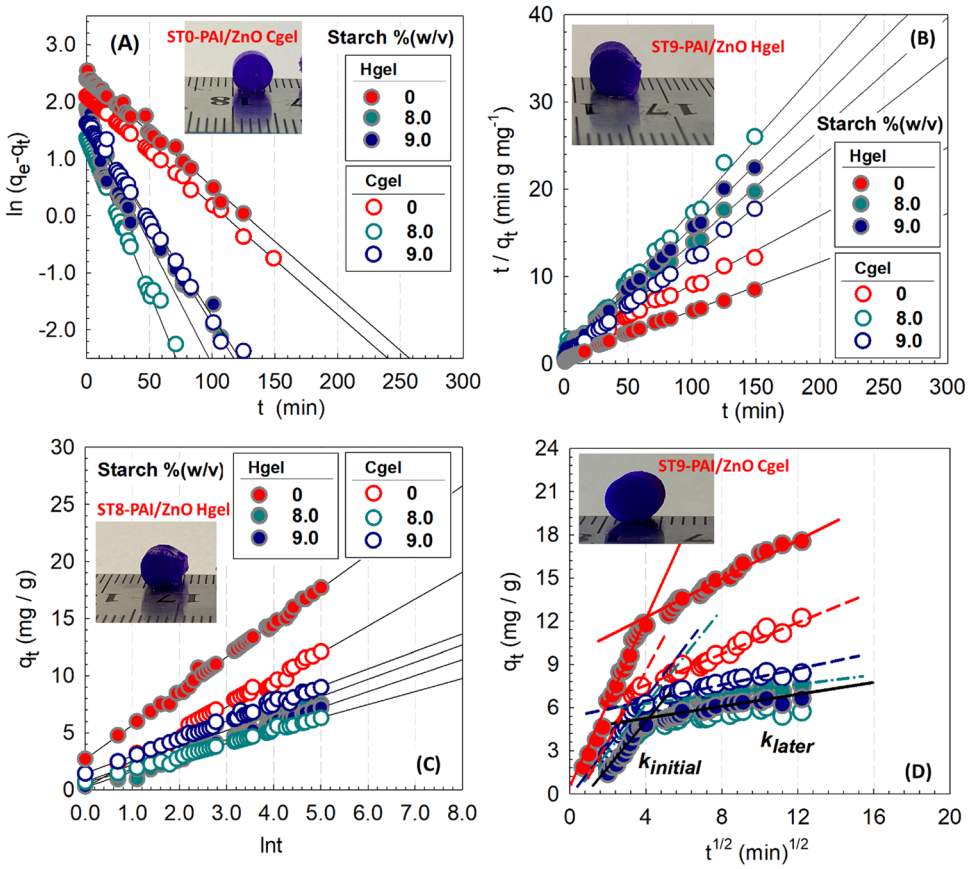

Fig. 11 Dye adsorption kinetics fitted with pseudo-first-order kinetic model (A), pseudo-second-order kinetic model (B), Elovich kinetic model (C), and dye adsorption mechanism fitted with intraparticle diffusion model (D). The solid line indicates the model fit in the experimental data. Dye concentration: 10 mg L^{-1}.

Various MV concentrations (10, 20, 30, 40, 50, and 100 mg L^{-1}) were used to analyze the effect of initial dye concentration on the adsorption capability of semi-IPN biocomposites. Fig. 12 shows the effect of the initial concentration of MV dye on the adsorption capacity of semi-IPN biocomposites. The optical images of semi-IPNs after adsorption in aqueous MV solutions with C_i = 10–100 mg L^{-1} are presented for comparison. The dye adsorption capacity increased initially with an increase in the MV concentration while the amount of the adsorbent was maintained constant. This is attributed to the greater availability of MV molecules in the vicinity of semi-IPN biocomposites. The increase in the dye concentration beyond 50 mg L^{-1}, however, did not affect significantly the adsorption capacity due to the saturation of surfaces of semi-IPNs. From Fig. 12, it can be seen that the adsorption of MV dye in different compositions of semi-IPN biocomposites corresponds to the S-type adsorption isotherms in the Giles classification system for the adsorption process. Scheme 2 presents an illustration of possible interactions between semi-IPN ST-PAI/ZnO gel and MV dye. The interactions between semi-IPN

Table 3 Kinetic parameters describing the adsorption of MV onto semi-IPN ST-PAI/ZnO Cgels prepared at different starch content based on pseudo-first-order, pseudo-second-order, Elovich, and intraparticle diffusion models

	Pseudo-first order model		Elovich model		
Starch (w/v)%	$k_1 \times 10^{-2}$ (min^{-1})	R^2	α (mg g^{-1} min^{-1})	β (g mg^{-1})	R^2
0	1.9817	0.9038	0.9861	0.4367	0.9431
8.0	5.4262	0.8906	0.9035	0.8924	0.9115
9.0	4.2651	0.8704	1.3715	0.6612	0.9423

	Pseudo-second order model		Intraparticle diffusion model			
Starch (w/v)%	$k_1 \times 10^{-2}$ (min^{-1})	R^2	$k_{initial}$ (mg g^{-1} $min^{-1/2}$)	R^2	$k_{later} \times 10^{-1}$ (mg g^{-1} $min^{-1/2}$)	R^2
0	0.5094	0.9858	3.3329	0.9807	0.5718	0.9634
8.0	2.3235	0.9944	1.5800	0.9881	0.1220	0.6633
9.0	1.5243	0.9978	1.9245	0.9624	0.2525	0.8812

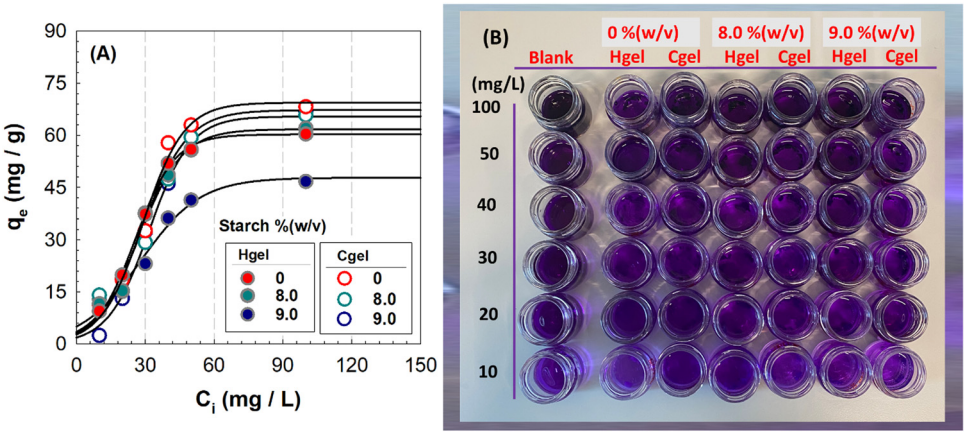

Fig. 12 (A) Effect of initial concentration of MV dye on adsorption capacity of semi-IPN ST-PAI/ZnO Hgels and Cgels. (B) Optical images of semi-IPN gels after adsorption in aqueous MV solutions with C_i = 10–100 mg L^{-1}.

biocomposites and MV molecules involve hydrogen bonding between hydroxyl groups of starch and MV, carboxylic groups of itaconic acid units, and N atoms of MV, and the electrostatic interaction between positive charge on MV and negative charges on semi-IPN biocomposite network. In order to explain the adsorption behavior of semi-IPN biocomposites against increasing initial MV dye concentrations, the four most known and applied adsorption isotherm models; Langmuir, Freundlich, Temkin and Dubinin–Radushkevich isotherm models were tested, and the constants of the obtained adsorption isotherm models were compared, as shown in Table 4. The plots of the tested isotherm models are presented in Fig. 13. The formulations of the linearized Langmuir and Freundlich isotherm models can be given as:

$$\frac{C_e}{q_e} = \frac{1}{q_{max} K_L} + \frac{C_e}{q_{max}} \quad \text{and} \quad R_L = \frac{1}{1 + K_L C_0} \tag{12a}$$

$$\ln q_e = \ln K_F + (1/n) \ln C_e \tag{12b}$$

where K_L is Langmuir adsorption equilibrium constant (L mg^{-1}), R_L is a dimensionless constant separation factor indicating the feasibility of adsorption. K_F is Freundlich adsorption equilibrium constant (mg g^{-1}) and parameter n is related to the adsorption capacity.

It is clear from Fig. 13(A) and Table 4 that the curves that best describe MV adsorption by semi-IPN biocomposites belong to the Langmuir isotherm in the linearized form, as confirmed by higher R^2 values. In this isotherm model, the adsorbent surface is considered to be similar in energy indicating a relatively uniform absorption surface with monolayer adsorption by keeping the MV dye in equal numbers, irreversible adsorption, and high compatibility. The dimensionless constant R_L for the affinity of semi-IPN biocomposites to MV dye obtained from Langmuir isotherm is used to predict whether the adsorption process is favorable or unfavorable. As R_L values are 0.9953–0.0104, this confirms the favorability of the adsorption process. The curves in Fig. 13(B) show the fitting results for the Freundlich model assuming that the adsorption is a multilayer process with heterogeneous and energetically

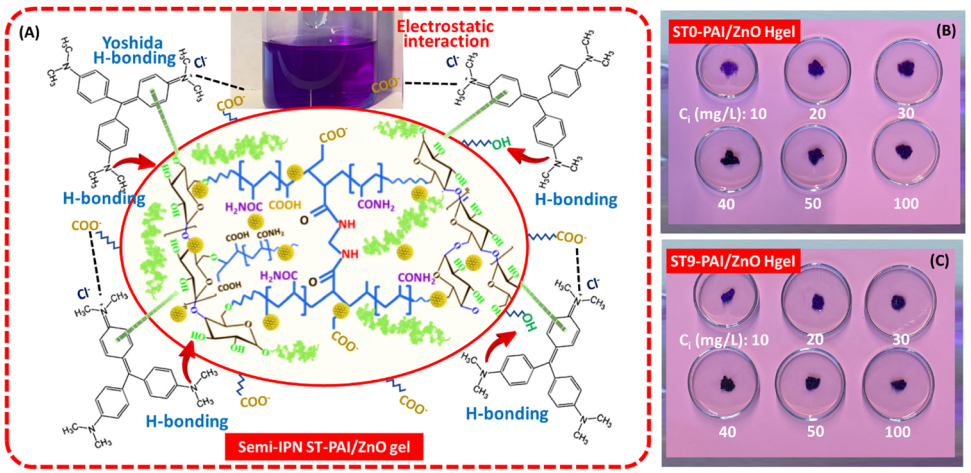

Scheme 2 (A) Illustration of the possible interactions between semi-IPN ST-PAI/ZnO gel and MV dye. (B) and (C) Optical images of the ST-free and 9.0% (w/v) of ST containing semi-IPN gels after adsorption in aqueous MV solutions with C_i = 10–100 mg L^{-1}.

Table 4 Variables of the linear Langmuir, Freundlich, Temkin and Dubinin–Radushkevich isotherm parameters for the adsorption of MV dye on semi-IPN ST-PAI/ZnO Hgels and Cgels containing different amounts of starch

		ST-PAI/ZnO Hgel			ST-PAI/ZnO Cgel		
Isotherm model	Isotherm parameters	0	8.0	9.0	0	8.0	9.0
Langmuir	K_L (L mg^{-1})	0.9750	0.1380	6.4942	2.2388	1.7167	0.0466
	R_L	0.9111–0.0127	0.9863–0.0103	0.6062–0.0286	0.8170–0.0164	0.8534–0.0149	0.9953–0.0104
	R^2	0.9110	0.8754	0.8892	0.9138	0.9266	0.9517
Freundlich	K_F (mg g^{-1})(mg L^{-1})$^{-1/n}$	2.7385	2.2545	4.0431	1.4815	3.6281	0.2155
	n_F	1.1580	1.0982	1.6613	0.8875	1.2809	0.6229
	R^2	0.7367	0.9769	0.8566	0.7652	0.7971	0.7520
Temkin	K_T (L mg^{-1})	0.3090	0.2577	0.3011	0.1981	0.2658	0.1729
	b_T (J mol^{-1})	107.51	95.028	160.77	69.542	96.655	85.021
	R^2	0.7367	0.9769	0.8566	0.7652	0.7971	0.7520
D–R	β (mol^2 kJ^{-2})	0.0588	0.1067	0.0558	0.1145	0.0553	0.1443
	E (kJ mol^{-1})	2.9142	2.2353	2.9929	2.0891	3.0056	1.8609
	R^2	0.7287	0.7641	0.7533	0.7697	0.7569	0.8237

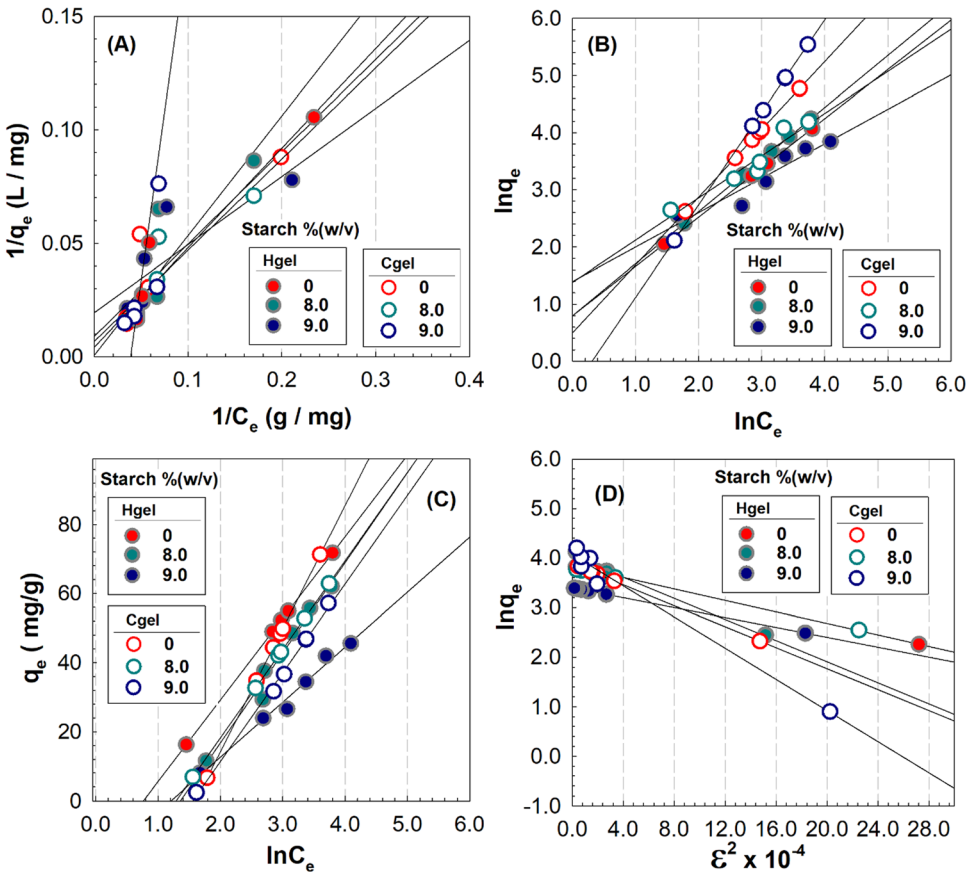

Fig. 13 Linear fitting of the isotherm models: Langmuir (A), Freundlich (B), Temkin (C) and Dubinin–Radushkevich (D) isotherms for the adsorption of MV to ST-PAI/ZnO Hgels and Cgels.

non-equivalent surface of the adsorbent. The comparison of R^2 parameters of the two models listed in Table 4 showed that the coefficients of the Langmuir model were much larger than that of the Freundlich model. In this model, the n value is an indicator of how good the adsorption performance will be. While high values indicate that adsorption occurs easily, the adsorption is considered difficult when $n < 0.5$. Taweekarn *et al.* reported the modeling of methylene blue (MB) adsorption onto tapioca starch biocryogels and the study showed that MB sorption was satisfactorily fitted by the Langmuir model rather than the Freundlich one, while the kinetics of MB adsorption on the cryogel followed a pseudo-second-order model.[61] In

another study, Taweekarn *et al.* reported the modeling of the kinetic data obtained from the removal of phosphate using calcium silicate hydrate composite starch cryogels.[62] Their fitting results using the Langmuir model indicated R_L values from 0.08 to 0.99 showing that the adsorption is favorable.

To test the adsorption of MV onto semi-IPN biocomposites, the linearized Temkin and Dubinin Radushkevich (D–R) isotherms were used in the following forms:

$$q_e = B_T \ln K_T + B_T \ln C_e \quad \text{and } B_T = \frac{RT}{b_T} \tag{13a}$$

$$\ln q_e = \ln q_{max} - \beta\varepsilon^2; \quad \varepsilon = RT \ln\left(1 + \frac{1}{C_e}\right); \quad E = \frac{1}{(-2\beta)^{1/2}} \tag{13b}$$

where B_T is the Temkin constant controlled by temperature, b_T (J mol^{-1}) is the model constant related to the heat of adsorption and K_T (L mg^{-1}) is the binding constant of Temkin isotherm related to maximum binding energy, ε is the Polanyi potential, and β is the D–R activity coefficient (mol^2 kJ^{-2}) related to the mean free energy of adsorption. According to the Temkin isotherm model, which suggests that the binding energies are uniformly distributed, the heat of adsorption decreases linearly when coverage is completed. Using this model, the values of B_T and K_T constants were determined from the slope and intercept achieved by plotting q_e against ln C_e, as shown in Fig. 13(C). The poor linearity with low R^2 values revealed the unsuitability of the Temkin model for describing adsorption for MV dye by the semi-IPN bicomposite surface. Gimbert *et al.* reported the modeling of the adsorption of an anionic dye, Acid Blue 25 sorption onto cationized starch-based adsorbent using Langmuir, Freundlich, Temkin, Generalized, Redlich–Peterson, and Toth isotherm models.[63] Although the values of $n > 1$ indicate favorable adsorption conditions, Langmuir isotherm has the highest R^2 values, whereas Freundlich and Temkin values were lower. The Langmuir model yielded a much better fit than the Freundlich model.

In Fig. 13(C), the linear form of the D–R isotherm model was illustrated to show the adsorption of MV dye onto semi-IPN biocomposites. D–R isotherm, which explains the distinction between chemisorption and physisorption, can explain the formation of multilayers. Since a homogeneous surface is not assumed in this model, it is more general than the Langmuir isotherm and therefore, at low coverage, this model can be used to describe the heterogeneity of the adsorbent surface. The activity coefficient β values shown in eqn (13b) were obtained from the intercept of the plot between ln q_e *versus* ε^2, as given in Fig. 13(D). Since the average free energy E values were less than 8 kJ mol^{-1}, the process could be physisorption, but the low correlation coefficients confirmed that the D–R isotherm was not suitable to describe the adsorption of MV dye when R^2 values are taken into account. Boughanmi *et al.* used this model for the adsorption of iron and sulfate ions onto starch and chitosan biopolymer.[64] Based on the Polanyi potential, it was reported that the sorption type was chemisorption since the E values varied between 56.14 and 68.94 kJ mol^{-1}.

Conclusions

To prepare the starch-embedded hybrid gels with good mechanical strength, two acrylic monomers AAm and IA were copolymerized in the presence of starch using BAAm as the chemical crosslinker *via* a common free radical polymerization using APS as the thermal initiator. A hybrid composite of ST-P(AAm-IA)/ZnO was synthesized to evaluate the effect of varying starch amounts on the swelling, architecture and mechanical properties. For both biocomposite hydrogels and cryogels, the swelling followed a decreasing order as copolymer PAI > starch-free PAI/ZnO > ST-PAI/ZnO gels. As starch was added to the PAI/ZnO structure, the swelling tended to decrease continuously. With the incorporation of 1% (w/v) ST, the swelling decreased by 36%, while with the addition of 9% (w/v) ST, the reduction was 84%. Examination of the compressive elastic behavior of semi-IPN biocomposites by uniaxial compression tests confirmed that the elastic properties strongly vary depending on the starch content. Increasing the amount of starch caused a significant increase in the elastic modulus, and this increase was observed more clearly in biocomposite cryogels. The compressive modulus of the cryogel bicomposite was higher than that of the hydrogel over the entire starch concentration range, indicating the stiffer network of the bicomposite cryogels. When compared to a fixed amount of starch, biocomposite cryogels exhibited significantly higher modulus than the hydrogels. The effective crosslinking density of semi-IPNs was presented by a cubic polynomial as a function of the starch content.

pH-induced swelling testing results showed that the swelling of ST-PAI/ZnO gels was highly dependent on pH, and as the pH increased, there was a gradual increase in the swelling ratio at two different pH values. Temperature-induced swelling testing showed that there was a decrease in the swelling of semi-IPN biocomposites with increasing external temperature, but a slight increase in the swelling was observed above 60 °C. The swelling studies showed that pH and starch content are basic parameters affecting the swelling of semi-IPN biocomposites. In buffer solutions of various pH, semi-IPN hydrogels and cryogels exhibited different swelling rates depending on the degree of ionization of the carboxylic acid groups of IA units. Semi-IPN biocomposite cryogels tended to swell at pH 11.2 due to anion–anion repulsive electrostatic forces and shrunk at pH 2.1 faster compared to hydrogels due to protonation of the carboxylate groups. The water absorbency increased sharply at the beginning of the swelling process in semi-IPN biocomposite cryogels, but slower initial swelling rates were observed in hydrogels, with slower swelling until equilibrium was reached. The swelling kinetics of semi-IPN biocomposites had high compliance with the second-order swelling kinetic model. The diffusion coefficients of semi-IPN biocomposite cryogels were higher than those of hydrogels, and this revealed that the incorporation of starch into the semi-IPN matrix resulted in faster penetration of water. It was analyzed whether they were effective adsorbents in the adsorption of methyl violet dye from aqueous solutions. The adsorption efficiency was investigated, and it was found that the pseudo-second-order and Langmuir

adsorption isotherm models well agreed with the adsorption behavior. Adsorption thermodynamics analysis showed the spontaneous nature of the adsorption with negative ΔG° values under normal conditions. Within the scope of this study, as it was aimed to provide a comprehensive understanding of the effectiveness and potential applications in wastewater treatment, the prepared semi-IPN bicomposites have desired swelling/elastic properties, high salt-response, good swelling kinetics in different pH solutions, and acceptable pH-dependent swelling reversibility, making these materials potential candidates for applications.

Conflicts of interest

There are no conflicts to declare.

Acknowledgements

This study was conducted by Istanbul Technical University, Institute of Science and Technology and supported as part of the PhD thesis by the Istanbul Technical University Research Fund.

References

1 H. Ismail, M. Irani and Z. Ahmad, *Int. J. Biol. Macromol.*, 2013, **62**, 411–420.
2 E. S. Dragan and D. F. Apopei, *Chem. Eng. J.*, 2011, **178**, 252–263.
3 X. Shang, Q. Wang, J. Li, G. Zhang, J. Zhang, P. Liu and L. Wang, *Carbohydr. Polym.*, 2021, **257**, 117626.
4 J. Jin, L. Cheng, C. Chen, Z. Li, Y. Hong, C. Li, X. Ban and Z. Gu, *Ind. Crops Prod.*, 2023, **196**, 116524.
5 A. Bora and N. Karak, *Eur. Polym. J.*, 2022, **176**, 111430.
6 A. Olad, F. Doustdar and H. Gharekhani, *Colloids Surf., A*, 2020, **601**, 124962.
7 W. Shao, P. Wang, J. Liu, H. Xu, X. Cai, Q. Wu, N. Xia and F. Kong, *Ind. Crops Prod.*, 2022, **181**, 114809.
8 A. V. Thanusha, A. K. Dinda and V. Koul, *Mater. Sci. Eng., C*, 2018, **89**, 378–386.
9 B. Kang, H. Tang, Z. Zhao and S. Song, *ACS Omega*, 2020, **5**(12), 6229–6239.
10 X. He and A. G. Ewing, *ChemBioChem*, 2023, **24**(9), e202200694, 1–9.
11 S. Ciftbudak and N. Orakdogen, *Colloids Surf., A*, 2022, **651**, 129756.
12 P. J. Flory, *Principles of polymer chemistry*, Cornell University Press, Ithaca, 1953.
13 B. Kalkan and N. Orakdogen, *Eur. Polym. J.*, 2022, **173**, 111296.
14 N. Orakdogen and O. Okay, *J. Appl. Polym. Sci.*, 2007, **103**, 3228–3237.
15 S. Ciftbudak and N. Orakdogen, *Polymer*, 2023, **266**, 125612.
16 R. P. Buck, S. Rondinini, A. K. Covington, F. G. K. Baucke, C. M. A. Brett, M. F. Camoes, M. J. T. Milton, T. Mussini, R. Naumann, K. W. Pratt, P. Spitzer and G. S. Wilson, *Pure Appl. Chem.*, 2002, **74**, 2169.
17 L. R. G. Treloar, *The physics of rubber elasticity*, University Press, Oxford, UK, 1975.
18 C. Pozo, S. Rodríguez-Llamazares, R. Bouza, L. Barral, J. Castaño, N. Müller and I. Restrepo, *J. Polym. Res.*, 2018, **25**, 266.
19 F. J. Warren, M. J. Gidley and B. M. Flanagan, *Carbohydr. Polym.*, 2016, **139**, 35–42.
20 H. Lu, R. Ma, R. Chang and Y. Tian, *Food Hydrocolloids*, 2021, **120**, 106975.
21 Y. K. Sun, Z. W. Wu, B. Hu, W. Wang, H. Ye, Y. Sun, X. Q. Wang and X. X. Zeng, *Carbohydr. Polym.*, 2014, **108**, 153–158.
22 X. Jiang, J. Liu, N. Xiao, X. Zhang, Q. Liang and W. Shi, *Food Biosci.*, 2024, **58**, 103675.
23 B. M. Keyes, L. M. Gedvilas, X. Li and T. J. Coutts, *J. Cryst. Grow.*, 2005, **281**(2–4), 297–302.
24 K. Sowri Babu, A. Ramachandra Reddy, C. Sujatha, K. Venugopal Reddy and A. N. Mallika, *J. Adv. Ceram.*, 2013, **2**(3), 260–265.
25 V. D. Mote, Y. Purushotham and B. N. Dole, *Mater. Des.*, 2016, **96**, 99–105.
26 W. Ma, L. Yang, Y. Wu, Y. Zhang, C. Liu, J. Ma and B. Sun, *RSC Adv.*, 2023, **13**(17), 11685–11696.
27 L. H. Li, J. C. Deng, H. R. Deng, Z. L. Liu and L. Xin, *Carbohydr. Res.*, 2010, **345**, 994–998.
28 P. Bindu and S. Thomas, *J. Theor. Appl. Phys.*, 2014, **8**, 123–134.
29 M. R. Arefi and S. Rezaei-Zarchi, *Int. J. Mol. Sci.*, 2012, **13**, 4340–4350.
30 M. Antony Lilly Grace, K. Veerabhadra Rao, K. Anuradha, A. Judith Jayarani, A. Arun kumar and A. Rathika, *Mater. Today Proc.*, 2023, **92**(2), 1334–1339.
31 C. Wang, J. Lv, Y. Ren, Q. Zhou, J. Chen, T. Zhi, Z. Lu, D. Gao, Z. Ma and L. Jin, *Carbohydr. Polym.*, 2016, **138**, 106–113.
32 D. Kundu and T. Banerjee, *Heliyon*, 2020, **6**, 1.
33 S. Keshavarzi, A. Babaei, A. Goudarzi and A. Shakeri, *Polym. Adv. Technol.*, 2019, **30**(4), 1083–1095.
34 A. Pourjavadi, S. H. Hosseini, F. Seidi and R. Soleyman, *Polym. Int.*, 2013, **62**, 1038–1044.
35 H. Hosseinzadeh and S. Ramin, *Int. J. Biol. Macromol.*, 2018, **106**, 101–115.
36 E. Motamedi, B. Motesharezedeh, A. Shirinfekr and S. M. Samar, *J. Environ. Chem. Eng.*, 2020, **8**(1), 103583.
37 A. Li, R. Liu and A. Wang, *J. Appl. Polym. Sci.*, 2005, **98**, 1351–1357.
38 R. Jia, C. Cui, L. Gao, Y. Qin, N. Ji, L. Dai, Y. Wang, L. Xiong, R. Shi and Q. Sun, *Carbohydr. Polym.*, 2023, **321**, 121260.
39 B. A. Macias-Rodriguez and K. P. Velikov, *Food Struct.*, 2022, **32**, 100257.
40 D. An, H. Li, D. Li, D. Zhang, Y. Huang, M. Obadi and B. Xu, *Food Chem.*, 2022, **393**, 133396.
41 J. Sringam, P. Pankongadisak, T. Trongsatitkul and N. Suppakarn, *Polymers*, 2022, **14**, 3552.
42 H. Kim, J. Kim and D. Kim, *Polymers*, 2021, **13**, 2859.
43 A. Martínez-Ruvalcaba, J. C. Sánchez-Díaz, F. Becerra, L. E. Cruz-Barba and A. González-Álvarez, *eXPRESS Polym. Lett.*, 2009, **3**(1), 25–32.

44 H. El-Hamshary, *Eur. Polym. J.*, 2007, **43**(11), 4830–4838.
45 J. C. Quintanilla de Stéfano, V. Abundis-Correa, S. D. Herrera-Flores and A. J. Alvarez, *Polymers*, 2020, **12**(9), 1974.
46 D. Soto, J. Urdaneta, K. Pernia, O. León, A. Muñoz-Bonilla and M. Fernández-García, *J. Polym. Environ.*, 2016, **24**, 343–355.
47 M. R. Jozaghkar, A. S. Azar and F. Ziaee, *Polym. Bull.*, 2022, **7**, 5183–5195.
48 Y. Sha and S. Adachi, *Food Sci. Technol. Res.*, 2015, **21**(4), 509–515.
49 A. D. Drozdov and J. deClaville Christiansen, *RSC Adv.*, 2020, **10**, 30723–30733.
50 C. S. Brazel and N. A. Peppas, *Eur. J. Pharm. Biopharm.*, 2000, **49**(1), 47–58.
51 J. Crank, *The Mathematics of Diffusion*, Clarendon Press, Oxford University Press, Ely House, London, WI, 1975.
52 H. Schott, *J. Macromol. Sci. Phys.*, 1992, **31**, 1–9.
53 X. Zhang, D. Guo, J. Xue, S. Yanniotis and I. Mandala, *Food Funct.*, 2017, **8**, 3792.
54 W. Wang, H. Zhou, H. Yang, S. Zhao, Y. Liu and R. Liu, *Food Chem.*, 2017, **214**, 319–327.
55 K. Junlapong, P. Maijan, C. Chaibundit and S. Chantarak, *Int. J. Biol. Macromol.*, 2020, **1**(158), 258–264.
56 J. Arayaphan, P. Maijan, P. Boonsuk and S. Chantarak, *Int. J. Biol. Macromol.*, 2021, **168**, 875–886.
57 H. Bakhshi and A. Darvishi, *Desalin. Water Treat.*, 2016, **57**(39), 18144–18156.
58 A. P. Nambiar, R. Pillai, M. Sanyal, Y. Vadikkeettil and P. S. Shrivastav, *Environ. Sci.: Adv.*, 2023, **2**, 861–876.
59 R. Bhattacharyya and S. K. Ray, *J. Ind. Eng. Chem.*, 2014, **20**, 3714–3725.
60 G. Sharma, M. Naushad, A. Kumar, S. Rana, S. Sharma, A. Bhatnagar, F. J. Stadler, A. A. Ghfar and M. R. Khan, *Process Saf. Environ. Prot.*, 2017, **109**, 301–310.
61 T. Taweekarn, W. Wongniramaikul, C. Boonkanon, C. Phanrit, W. Sriprom, W. Limsakul, W. Towanlong, C. Phawachalotorn and A. Choodum, *Polymers*, 2022, **14**, 5543.
62 T. Taweekarn, W. Wongniramaikul and A. Choodum, *J. Environ. Manage.*, 2022, **301**, 113923.
63 F. Gimbert, N. Morin-Crini, F. Renault, P.-M. Badot and G. Crini, *J. Hazard. Mater.*, 2008, **157**(1), 34–46.
64 R. Boughanmi, C. Steinbach, N. Gerlach, M. Oelmann, C. Beutner and S. Schwarz, *Polysaccharides*, 2023, **4**, 325–342.